nature neuroscience

Divergence of visual channels in the inner retina

Hiroki Asari[1,2] & Markus Meister[1,2]

Bipolar cells form parallel channels that carry visual signals from the outer to the inner retina. Each type of bipolar cell is thought to carry a distinct visual message to select types of amacrine cells and ganglion cells. However, the number of ganglion cell types exceeds that of the bipolar cells providing their input, suggesting that bipolar cell signals diversify on transmission to ganglion cells. We explored in the salamander retina how signals from individual bipolar cells feed into multiple ganglion cells and found that each bipolar cell was able to evoke distinct responses among ganglion cells, differing in kinetics, adaptation and rectification properties. This signal divergence resulted primarily from interactions with amacrine cells that allowed each bipolar cell to send distinct signals to its target ganglion cells. Our findings indicate that individual bipolar cell–ganglion cell connections have distinct transfer functions. This expands the number of visual channels in the inner retina and enhances the computational power and feature selectivity of early visual processing.

The visual system processes light information by encoding and separating signals into many different channels. These operations begin in the bipolar cells of the retina[1]. Bipolar cells are the secondary neurons, extending their dendrites and axons toward the outer and inner retina, respectively, and they constitute the only conduit for transmitting the signals from photoreceptors to retinal ganglion cells and amacrine cells[2]. There are ~10 types of bipolar cells in a vertebrate retina[3,4], and previous studies have suggested that they form parallel channels in which each bipolar cell type carries a distinct type of visual information[5]. Bipolar cells differ in morphology, in particular by the ramification pattern of dendrites[6] and the stratification of axonal arbors[3,4]. They have also been divided physiologically into ON and OFF response types, and, in each of these groups, one further distinguishes between 'transient' and 'sustained' types on the basis of their visual response characteristics[7]. Such functional differentiation results from connections to specific photoreceptors[8], the intrinsic properties of bipolar cells, such as their membrane receptors and channels[9,10], and inhibitory circuitry involving amacrine cells in the inner retina[11–13].

Beyond separating the visual image into parallel channels, bipolar cells carry out important roles through their transmission to ganglion cells[1,14]. First, some bipolar cell synapses appear to be strongly rectifying, transmitting depolarization, but not hyperpolarization, which leads to prominent nonlinearities in the responses of ganglion cells, such as a pronounced sensitivity to pattern motion[15–17]. Other ganglion cells respond more linearly[18], presumably drawing on bipolar cell synapses with less rectification. Second, some important nonlinearities arise through the interaction with amacrine cells at the bipolar cell terminal. For example, the direction selectivity of ganglion cells is largely determined by presynaptic inhibition of bipolar cell inputs[19]. Finally, bipolar cell synapses can undergo strong activity-dependent depression[20–23], and this short-term plasticity has been invoked as a mechanism for adaptation in certain ganglion cell responses[14,24]. Thus, the function of bipolar cell–ganglion cell transmission has emerged as a key determinant of retinal computation.

The diversity of functions that have been assigned to bipolar cells, a combination of stimulus filtering, nonlinearities and plasticity, easily exceeds the number of distinct bipolar cell pathways. Indeed, the typical retina contains ~20 types of ganglion cells[2]. Because each of the ten bipolar cell types tiles the visual field with little overlap[25], a complete coverage by ganglion cells therefore requires divergence from individual bipolar cells to multiple ganglion cells. This raises the question of how those bipolar cell signals become diversified.

To address this issue, we studied divergence and convergence of transmission from bipolar cells to ganglion cells. We gained control of individual bipolar cells in the salamander retina with sharp electrodes; simultaneously, we recorded the firing in an entire field of surrounding ganglion cells with an extracellular multielectrode array. In addition, we modulated the amacrine cell network pharmacologically and stimulated the photoreceptors with patterns of light. We found that individual bipolar cells distributed very distinct signals to different ganglion cells. Interactions with amacrine cells were essential for diversifying the temporal dynamics and adaptation properties of the signals, but not for other characteristics such as the degree of rectification. We also found that different outputs from each bipolar cell were modulated individually by amacrine cells; thus, signals to some target ganglion cells were suppressed while those to others were unaffected or even enhanced by disinhibition. Taken together, our results suggest that visual information undergoes marked divergence and convergence during transmission in the inner retina and that considerable computation takes place at each bipolar cell–ganglion cell connection.

RESULTS

To explore how each bipolar cell signal is distributed downstream, we intracellularly manipulated the activity of individual bipolar cells in

[1]Department of Molecular and Cellular Biology and Center for Brain Science, Harvard University, Cambridge, Massachusetts, USA. [2]Present address: Division of Biology, California Institute of Technology, Pasadena, California, USA. Correspondence should be addressed to M.M. (meister@caltech.edu).

Received 27 June; accepted 20 September; published online 21 October 2012; doi:10.1038/nn.3241

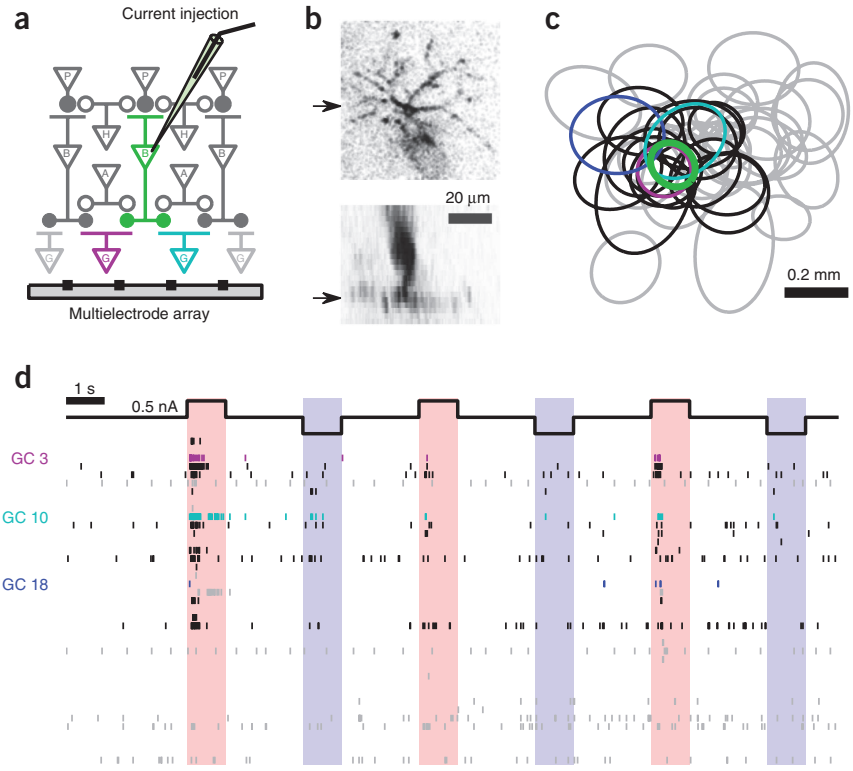

Figure 1 Many ganglion cells respond to input from a single bipolar cell. (**a**) Schematic diagram of the experiment. A single bipolar cell was impaled with a sharp electrode and intracellularly stimulated by current injection (see **d** for example) while a population of ganglion cells (GCs) was simultaneously recorded with a multielectrode array. Filled circles represent excitatory synapses and open circles represent inhibitory synapse. A, amacrine cell; B, bipolar cell; G, ganglion cell; H, horizontal cell; P, photoreceptor. (**b**) Horizontal view of a bipolar cell, focusing on the axon arbors in the inner plexiform layer (top) and the vertical view across the soma (bottom). The arrows indicate locations of the image slices shown in the other panels. (**c**) The receptive field centers of an intracellularly recorded bipolar cell (green) and 39 ganglion cells on the electrode array (gray, unconnected; black, cyan, purple and blue, connected; see **d** for connectivity analysis). Each outline represents a two-dimensional Gaussian fit to the receptive field profile (contour at 1 s.d.; see **Supplementary Fig. 1**). (**d**) Raster graph of ganglion cell spikes in response to inputs from a single bipolar cell (from **c**). Each row represents the spiking activity of a single ganglion cell, arranged in order of increasing distance from the bipolar cell (top to bottom). Either depolarizing (pink-shaded periods) or hyperpolarizing (blue-shaded periods) current pulses were delivered to the bipolar cell intracellularly (top trace, only the first three trials are shown; see **Supplementary Fig. 1**). The three representative ganglion cells from **c** are shown in the respective colors.

the isolated salamander retina (**Fig. 1a**,**b**) and simultaneously recorded the spiking activity of many surrounding ganglion cells (**Fig. 1c**,**d**). Depolarization of a bipolar cell via current injection frequently elicited spikes in nearby ganglion cells (**Fig. 1d**), including those of different cell types (**Supplementary Fig. 1**). These sign-preserving responses in ganglion cells likely arise via excitatory transmission from bipolar cells. Other ganglion cells were inhibited by bipolar cell depolarization, and we confirmed by pharmacological block of inhibition that this sign inversion arose from interposed amacrine cells (**Supplementary Fig. 2**). Although it is reassuring that the actions of a single bipolar cell can be measured even across intervening neurons, we focused on sign-preserving transmission to ganglion cells.

Some of the sign-preserving responses were observed at great distances, up to ~1 mm from the stimulated bipolar cell. Given that the combined radius of bipolar cell terminal fields and ganglion cell dendritic fields is ~0.35 mm[3,26,27], these effects cannot arise from a monosynaptic connection. Such long-range connections were greatly attenuated when we applied a gap junction blocker (**Supplementary Fig. 1**), suggesting that signals propagate laterally through electrical junctions among neurons in the inner retina[26,28]. To exclude such patently polysynaptic effects, we further restricted the analysis to cell pairs separated by ≤0.35 mm.

With these methods in place, we set out to characterize the diversity of signal transmission from bipolar cells to ganglion cells. For the reasons detailed above, we focused the approach on four aspects of bipolar cell–ganglion cell connections: the dynamics of the ganglion cell response, adaptation in ganglion cell responses across repeated bipolar cell depolarizations, rectification of signal transmission to ganglion cells and the gating of bipolar cell–ganglion cell signaling by amacrine cells. All relationships described as significant were statistically significant at the $P < 0.05$ level.

Dynamics

By examining the postsynaptic responses, we found considerable divergence and convergence of distinct bipolar cell signals. First, the same bipolar cell was able to evoke very different ganglion cell responses. For example, depolarization of a single bipolar cell elicited a sustained response in one ganglion cell and a sharply transient response in another (**Fig. 2a**). This indicates that the signals acquire their distinct dynamics at or after the bipolar cell–ganglion cell transmission. Second, a single ganglion cell was able to produce distinct responses to inputs from different bipolar cells. After serially impaling several bipolar cells, we encountered some ganglion cells with a sustained response to one bipolar cell, but a transient response to another bipolar cell (**Fig. 2b**). This indicates that the distinct dynamics arise at or before the bipolar cell–ganglion cell transmission. Apparently, the transmission dynamics are specified neither by the presynaptic bipolar cells nor by the postsynaptic ganglion cells, but are instead determined at each individual bipolar cell–ganglion cell connection.

How substantial is this diversity in the output from individual bipolar cells? To assess this quantitatively, we examined the time course of ganglion cell firing on bipolar cell depolarization for each bipolar cell–ganglion cell connection. We found that more than two-thirds of all bipolar cells had significant variation in the peak latency among their connections to target ganglion cells (**Fig. 2c**). Furthermore, the variation among the outputs from a single bipolar cell explained about two-thirds of the total variation across all of the bipolar cell–ganglion cell connections. Given that the bipolar cells were sampled blindly from all cell types by the sharp electrode, it appears that the variation across cell types is less substantial than the variation across the outputs of a single bipolar cell. Similarly, many ganglion cells showed diversity among their bipolar cell inputs (**Fig. 2d**).

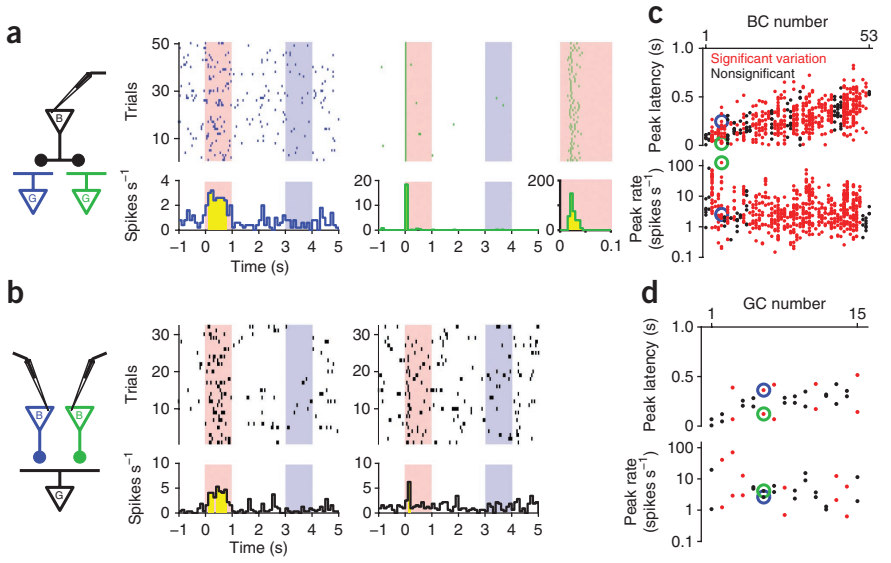

Figure 2 Individual pairs of bipolar and ganglion cells have distinct transmission properties. (**a**) Responses of two ganglion cells (top, raster graphs; bottom, peri-stimulus time histogram (PSTH); yellow bins, significant deviation from spontaneous firing rate) to current stimulation of a single bipolar cell. Current stimuli are color coded (pink and blue) as in **Figure 1d**. Note the sustained firing in one ganglion cell (left) and very transient firing in another (middle, magnified at right). (**b**) Responses of a single ganglion cell to current stimulation of two different bipolar cells (left and right; displayed as in **a**). (**c**) Population data for synaptic connections divergent from the same bipolar cell. Each dot represents one bipolar cell–ganglion cell connection (one column for each bipolar cell, BC). Top, peak latency evoked by bipolar cell depolarization (0.28 ± 0.15 s, mean ± s.d. from 633 ganglion cell responses). Significant variation was found in ganglion cell responses to 38 out of 53 bipolar cells (red). The variation among the connections of individual bipolar cells explained 62% of the total variation, whereas the variation across different bipolar cells explained only 38% (see Online Methods). Bottom, for the peak firing rate (6.6 ± 11.0 spikes s^{-1}), significantly different ganglion cell responses were found in 43 bipolar cells. The variation among connections from the same bipolar cell explained 67% of the total variation. (**d**) Population data for synaptic connections convergent on the same ganglion cell (displayed as in **c**). Inputs from different bipolar cells were able to drive the same ganglion cell differently (5 of 15 ganglion cells for peak latency, 6 ganglion cells for peak rate) and distinct dynamics could arise even with the same evoked firing rate (as in **b**, indicated by blue and green circles).

Visual signals therefore differentiate in their dynamics not only at bipolar cell dendrites in the outer retina[7,10], but also on transmission from bipolar cells to ganglion cells in the inner retina, and before they are integrated by the ganglion cells. This may involve a combination of pre- and postsynaptic mechanisms that are private to the individual bipolar cell–ganglion cell connections. One explanation of such diversity involves the function of inhibitory interneurons. For example, the transient responses could arise as a result of feedback or feedforward inhibition via amacrine cells[11–13]. Another possible explanation is that individual synapses have different pre- or postsynaptic mechanisms, for instance, by using different receptor types[29,30]. We distinguished these alternatives by pharmacological methods (**Fig. 3**). Following a block of inhibitory transmission via GABA and glycine, the peak evoked firing rates increased in almost all of the ganglion cells (**Fig. 3c**), as would be expected from a general loss of inhibition. This was accompanied by changes in the dynamics of the response. Unexpectedly, however, the dynamics of transient and sustained responses were altered in opposite directions. Following the inhibitory block, the formerly transient responses peaked later (**Fig. 3a**), whereas the formerly sustained responses peaked earlier (**Fig. 3b**). Thus, the overall diversity in the ganglion cell response kinetics evoked by single bipolar cells decreased significantly after elimination of amacrine cell circuits (**Fig. 3d**).

How can these bidirectional changes in dynamics be explained? Given the large increase in the evoked firing rate, one would generally expect a faster decline of the response as a result of synaptic fatigue, and therefore a shorter time to peak (**Fig. 4**). For example, because tonic presynaptic inhibition prevents synaptic depletion[20,21,31,32], the pharmacological block of such inhibition would speed up the postsynaptic ganglion cell response to bipolar cell depolarization (**Fig. 4b**). But clearly this is not the only effect at work, as the formerly transient responses became more extended in time. One explanation for transient responses is that feedback or feedforward inhibition can truncate synaptic transmission shortly after onset of the ganglion cell response[11–13]. With such a microcircuit at the bipolar cell–ganglion cell connection, the loss of inhibition will lead to a longer peak latency (**Fig. 4a,c**). From these results, it appears that distinct microcircuits with inhibitory amacrine cells are involved in regulating the dynamics of individual bipolar cell–ganglion cell connections and that even a single bipolar cell engages quite different amacrine cell microcircuits at its various synapses.

Adaptation

Following repeated exposure to the same stimulus, many ganglion cells change their response properties over time. Previous studies have suggested that events at the bipolar cell terminal contribute to these visual adaptations in ganglion cell responses[22–24]. We therefore examined whether ganglion cell responses evoked by single bipolar cell inputs change over consecutive trials (**Fig. 5**). Specifically, we alternately delivered 1 s of depolarizing and hyperpolarizing currents into individual bipolar cells with 2-s intervals (**Fig. 1d**) and analyzed slow changes in the peak rate and latency of the ganglion cell responses. To avoid confusion between spontaneous and evoked spikes, we selected those ganglion cells that had low spontaneous firing rates (≤1 Hz) and high evoked rates (≥5 Hz).

In the course of many repeated trials, some ganglion cells desensitized, in that their responses became weaker and slower (**Fig. 5a**). In contrast, responses of other ganglion cells did not change significantly (**Fig. 5b**), even though they all received inputs from the same bipolar cell. Notably, slow changes in the peak rate or in the latency were able to occur independently of each other (**Fig. 5c,d**). Compiling results from many such experiments resulted in a view of the broad diversity of adaptive behaviors, including both desensitization and sensitization, even in transmission from a single bipolar cell. Indeed, the variation arising among the connections of individual bipolar cells explained most of the total variation in the adaptive behavior of the response latency, and about two-thirds of the variation in the changes of the peak rate (**Fig. 5e**).

To examine the contribution of amacrine cell circuits, we again blocked inhibitory synaptic transmission pharmacologically.

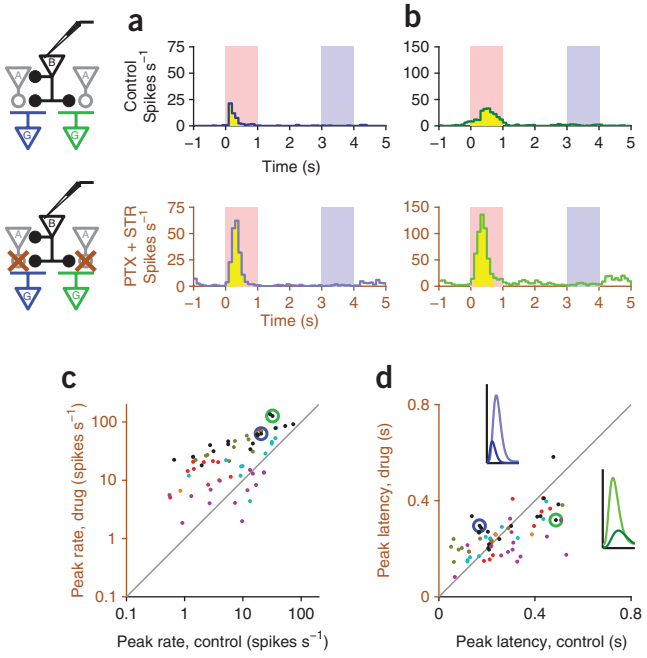

Figure 3 Dynamics of bipolar cell signals are diversified by amacrine circuits. (**a**,**b**) Spiking response of two ganglion cells to current stimulation of a bipolar cell, with (top) and without (bottom) inputs from amacrine cells. After blocking amacrine cell signals with 100 µM picrotoxin (PTX) and 1.0 µM strychnine (STR), the transient burst of spikes in one ganglion cell became considerably stronger and peaked later (**a**), whereas the sustained response in the other ganglion cell became stronger, but peaked earlier (**b**). (**c**,**d**) Summary of the effects of blocking inhibitory synaptic transmission on the peak firing rate (**c**) and the peak latency (**d**) evoked by single bipolar cell depolarization. Scatter plots comparing the ganglion cell responses with (abscissa) and without (ordinate) inhibitory transmission (66 ganglion cells in total from 6 bipolar cells indicated by different colors; blue and green circles indicate those shown in **a** and **b**, respectively) are shown. With the inhibitory circuits active, the peak firing rate was lower (**c**; $P < 0.001$, sign-test; control, 12.4 ± 13.7 spikes s^{-1}; drug, 32.7 ± 29.1 spikes s^{-1}; mean ± s.d.), but there was a greater range in the peak latency (**d**; $P < 0.001$, Levene's test; control, 0.27 ± 0.13 s; drug, 0.26 ± 0.09 s). In all six experiments, blocking amacrine cell signals made sustained responses more transient and transient responses more sustained. Insets in **d** correspond to curve fits for the examples in **a** (dark and light blue) and **b** (dark and light green).

We found that the sensitizing or stable responses were largely turned into desensitizing ones (**Fig. 5f**,**g**): almost all bipolar cell–ganglion cell connections showed a gradual decline in the peak firing rate, with less diversity than before the block. Again, it appears that diverse amacrine cell circuits are responsible for much of the variation in behavior of bipolar cell–ganglion cell connections, even on the slow timescale of adaptation.

Although these results indicate diverse adaptive behaviors among the output connections of one bipolar cell, does the same diversity apply among the inputs of a given ganglion cell? For example, an inactivating sodium conductance contributes to slow desensitization at the level of spike generation[33,34], which should affect every bipolar cell input to that ganglion cell equally. Similarly, the sensitizing responses of certain ganglion cells have been explained with a circuit model that affects all of the bipolar cell inputs[35]. To test this notion, we drove the same ganglion cell by stimulating two different bipolar cells intracellularly (**Fig. 6**). We found multiple cases in which the ganglion cell adapted to inputs from one bipolar cell, but not to those from another bipolar cell (**Fig. 6b**), even though the nonadapting responses were sometimes stronger than the adapting ones (**Fig. 6a**).

To further examine whether adaptation to inputs from one bipolar cell occurs independently of the other, we drove a single bipolar cell with current injection and many other bipolar cells with a visual stimulus presented far from the impaled bipolar cell (**Fig. 6c–e**). Over a 10-s train of current pulses into the single bipolar cell, most ganglion cells desensitized strongly (**Fig. 6d**), and the response often vanished completely (**Fig. 6c**). If this adaptation originated in a general loss of sensitivity after the ganglion cell integrates its synaptic currents[33,34], it should affect the response to all of the bipolar cell inputs. Instead, the ganglion cell responses to the light-evoked bipolar cell pathway did not change at all (**Fig. 6e**). This suggests that the adaptation arises in the input pathway from a single bipolar cell. Combined with the

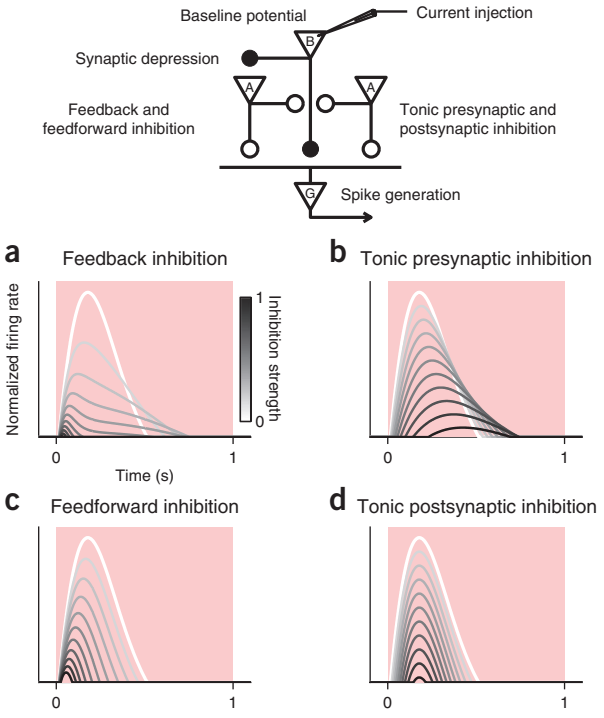

Figure 4 Interactions with amacrine cells can control the kinetics of connections between bipolar and ganglion cells. (**a**–**d**) We simulated how a step change in the input current to a bipolar cell is transduced into an evoked ganglion cell firing rate in the presence of four distinct types of amacrine cell inputs (see circuit diagram at top and Online Methods): tonic presynaptic inhibition of the bipolar cell terminal (**b**), tonic postsynaptic inhibition of the ganglion cell (**d**), feedback presynaptic inhibition (**a**) and feedforward postsynaptic inhibition (**c**). For all four types of inhibitory interactions, the evoked firing rate decreases as the inhibitory effects become stronger (trace color from white to black; see **Supplementary Fig. 3** for the effects of bipolar cell baseline potential). However, the effects on the response kinetics varied (compare with experiments in **Fig. 3**). Tonic presynaptic inhibition prevented synaptic depletion, thereby extending the ganglion cell response in time (**b**). Tonic postsynaptic inhibition affected the spiking threshold, but not the release dynamics, of bipolar cell terminals. Thus, the peak latency remained unchanged (**d**). Both feedback presynaptic inhibition (**a**) and feedforward postsynaptic inhibition (**c**) shortened the ganglion cell responses by truncating the later component of the excitation. They differed, however, in that presynaptic inhibition slowed vesicle release and therefore prevented rapid synaptic depression, producing weaker, but prolonged, postsynaptic responses over an intermediate regime.

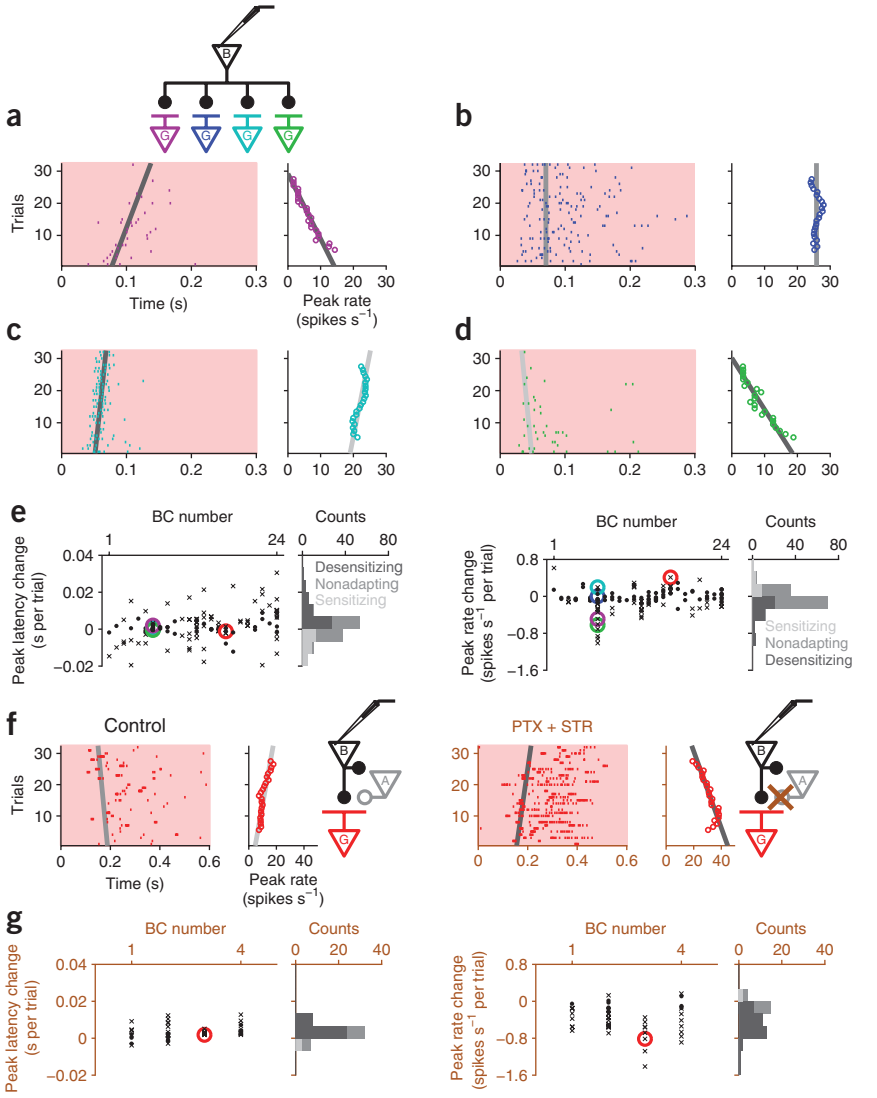

Figure 5 Adaptation of bipolar cell signals depends on interaction with amacrine cells. (**a**–**d**) Responses of four simultaneously recorded ganglion cells to depolarization of a single bipolar cell and their evolution over trials. (**a**) Left, raster graph showing spikes during the first 300 ms of depolarizing current, delivered in many successive 6-s-long trials (**Fig. 1d**); gray line is a linear fit to the peak latency over trials (gray, nonsignificant change; dark gray, significant increase or desensitization; light gray, significant decrease or sensitization). Right, variation of the peak firing rate over trials with a linear fit. (**b**–**d**) Responses of three additional ganglion cells with different characteristics (displayed as in **a**). (**e**) Population data for the slow changes in the peak latency (left) and peak rate (right). Each data point represents the adapting behavior of one bipolar cell–ganglion cell connection, estimated by the slopes of the linear fits as in **a**–**d** (cross, significant change; dot, nonsignificant change; colored circles indicate those from **a**–**d** and **f**). Each column shows the connections of one bipolar cell (sorted in order of increasing mean latency changes). The stacked histograms were obtained from 129 bipolar cell–ganglion cell connections in total (gray, nonsignificant change; dark gray, significant desensitization; light gray, significant sensitization). For latency adaptation, 20 out of 24 bipolar cells showed significant variation among their connections to ganglion cells, and this variation originating from individual bipolar cells explained 85% of the total variation. For peak rate adaptation, 14 bipolar cells showed significant variation and that accounts for 59% of the total. (**f**) Spiking responses of a ganglion cell to bipolar cell depolarization before (left) and after (right) pharmacological block of amacrine cell signals by 100 µM picrotoxin (PTX) and 1.0 µM strychnine (STR). Data are presented as in **a**–**d**. (**g**) Population data (57 ganglion cells total) for the adapting changes in the peak latency and peak rate over trials in absence of amacrine cell transmission (displayed as in **e**). After the block of amacrine cell signals, ganglion cells showed desensitization more frequently for both the latency ($P < 0.002$, χ^2 test) and the peak rate ($P < 0.002$, χ^2 test).

above results on divergence from a single bipolar cell, we conclude that desensitization and sensitization are specific to a given bipolar cell–ganglion cell connection and are not attributable to global changes in either the presynaptic or postsynaptic neuron.

Rectification

Under stimuli of moderate strength, bipolar cell responses can be well described by a linear function of the light intensity[36,37]. In contrast, many ganglion cells show highly nonlinear responses under these same stimulus conditions[15,16], and this effect has been attributed to rectification at the transmission from bipolar cells to ganglion cells[14,17]. Indeed, we generally found a strong asymmetry in ganglion cell responses (**Fig. 2**): bipolar cell depolarization excited the ganglion cell much more than hyperpolarization inhibited it. Because many ganglion cells had low spontaneous firing rates, however, this asymmetry could be a result of a cellular nonlinearity of spike generation in the ganglion cell rather than synaptic rectification. To focus on the bipolar cell–ganglion cell transmission properties, we selected ganglion cells with sufficiently high spontaneous firing rates (≥1 Hz) so that we could resolve a decrease, as well as an increase, in the firing rates. For those ganglion cells, we examined the effects of bipolar cell currents of either polarity and asked whether the transmission was rectified or not. To this end, we used a rectification index that measures the relative efficacy of bipolar cell depolarization and hyperpolarization in changing the ganglion cell spiking activity (see Online Methods).

In general, bipolar cell depolarization and hyperpolarization had opposite effects on any given ganglion cell (**Fig. 7**); one led to an increase of the firing rate and the other to a decrease. However, the relative strength varied over a wide range (**Fig. 7b**). For some ganglion cells, only bipolar cell depolarization was effective (**Fig. 7a**), suggesting a rectifying transmission with the index distributed around unity. In others, depolarization and hyperpolarization had comparable effects in opposite directions (**Fig. 7a**), indicating nonrectifying transmission with an index close to zero. For nonrectifying connections, we frequently observed rebound responses, an increase in firing at the offset of bipolar cell hyperpolarization, whereas we only rarely observed these for rectifying

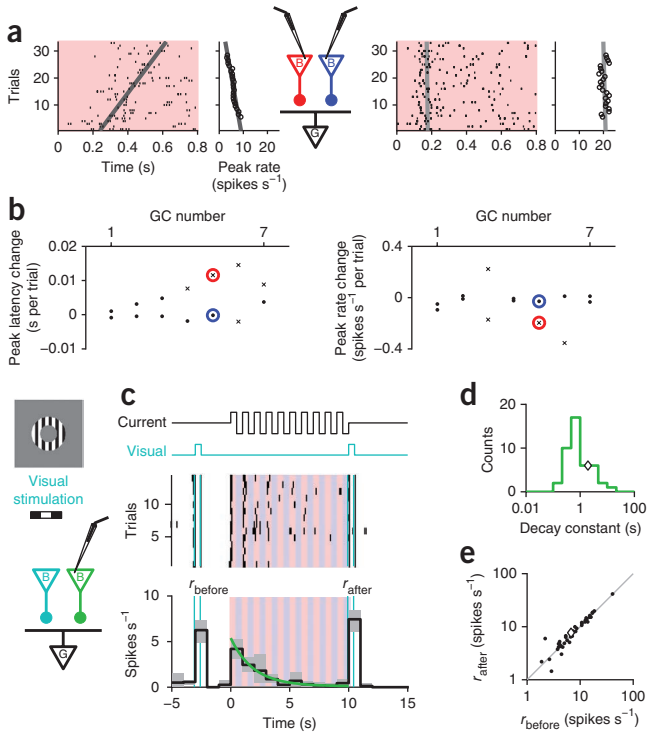

Figure 6 Adaptation is specific to individual pairs of bipolar and ganglion cells. (**a**) Responses of a single ganglion cell to depolarization of two different bipolar cells (displayed as in **Fig. 5a**). The response to one bipolar cell showed strong desensitization over time (left), whereas that to another bipolar cell did not, despite a higher peak firing rate (right). (**b**) Population data for the slow changes in peak firing rate and latency evoked by depolarization of two different bipolar cells (displayed as in **Fig. 5e**, colored circles indicate those shown in **a**). Inputs from different bipolar cells led to different adapting behaviors in the same ganglion cells (four of seven ganglion cells for the peak latency change, three ganglion cells for the peak rate change). (**c**) Responses of a ganglion cell to two different inputs: current injected into a bipolar cell (top, black trace) and visual stimulation in an annulus that did not drive the injected bipolar cell (cyan, contrast-reversing grating). The ganglion cell fired on bipolar cell depolarization (middle, raster graph). This response declined over subsequent current stimulations (bottom, PSTH; gray, 95% confidence interval; green, single exponential fit). The ganglion cell also fired on the visual stimulation, both before (r_{before}) and after (r_{after}) the current injection. (**d**,**e**) Results from many such experiments (6 bipolar cells and 44 ganglion cells; diamonds indicate the example shown in **c**). Most ganglion cells showed desensitization in response to consecutive bipolar cell depolarizations (**d**, histogram of decay constants for an exponential fit as in **c**). This, however, did not affect the ganglion cell's responses to other bipolar cells driven by the visual stimulus (**e**, $P > 0.06$, sign test).

connections (**Supplementary Fig. 3**). Because a given bipolar cell can make both rectifying and nonrectifying transmission to different targets (**Fig. 7a**), that same neuron can contribute to fundamentally different visual computations. We found that ~40% of the total variation of the rectification index arose from the diversity among the outputs from individual bipolar cells (**Fig. 7b**).

Blocking inhibitory transmission did not affect the degree of rectification in bipolar cell–ganglion cell connections. Neither the rectification index nor the observed frequency of rectifying and nonrectifying responses changed significantly following the pharmacological block (**Fig. 7b**,**d**). Even without the contribution of amacrine cells, the same bipolar cell could therefore send both rectified and nonrectified signals to different ganglion cells (**Fig. 7c**). This indicates that the signal rectification is intrinsic to individual bipolar cell–ganglion cell connections, perhaps depending on the baseline levels of calcium and vesicle release rates at the presynaptic bipolar cell terminals[38,39] (**Supplementary Fig. 3**).

Gating

We observed that signals from amacrine cells can strongly affect transmission at individual bipolar cell–ganglion cell connections (**Figs. 3–5**). In the experiments described thus far, these amacrine cell signals were only evoked by the intracellularly stimulated bipolar cell. In general, amacrine cells receive stimulation from a broader region of

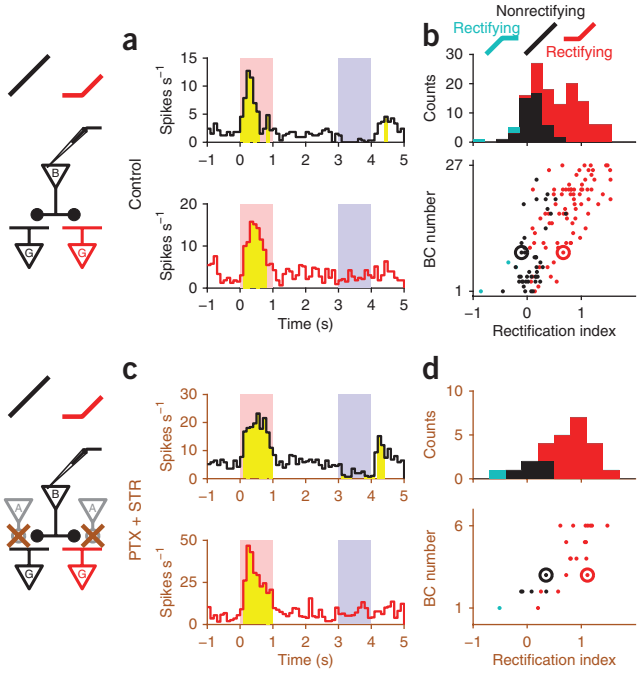

Figure 7 Rectifying and nonrectifying transmission from bipolar cells. (**a**) Response of two simultaneously recorded ganglion cells to current injection of a single bipolar cell. One ganglion cell responded to both bipolar cell depolarization and hyperpolarization with opposite sign (top, nonrectifying transmission, black) and showed a rebound response at the end of the hyperpolarization (**Supplementary Fig. 3**). In contrast, the other ganglion cell responded only to the depolarization (bottom, rectifying transmission, red) and did not show the rebound response. (**b**) Population results of rectification index from many such paired recordings (0.50 ± 0.48, mean ± s.d. from 127 ganglion cells, see Online Methods). Bottom, each dot represents one bipolar cell–ganglion cell connection (black and red circles from **a**) and each row corresponds to one bipolar cell. Top, stacked histogram across all bipolar cell–ganglion cell connections (black, nonrectifying connections; red and cyan, rectifying connections transmitting primarily on bipolar cell depolarization or on hyperpolarization, respectively). Both types of connections were found in ganglion cell responses to 17 of 27 bipolar cells (such as in **a**). The variation of the index in individual bipolar cells accounted for 41% of the total variation. (**c**) Response of two ganglion cells to a single bipolar cell under pharmacological block of inhibitory transmission (data are presented as in **a**, but for a different pair of cells). (**d**) Population results of rectification tested without amacrine cell signaling (25 ganglion cells in total). Despite an increase in the evoked firing rates (**Fig. 3c**), the inhibitory transmission blockers did not significantly change the rectification index ($P > 0.06$, rank sum) or the observed frequencies of rectifying and nonrectifying connections across the populations ($P > 0.6$, χ^2 test).

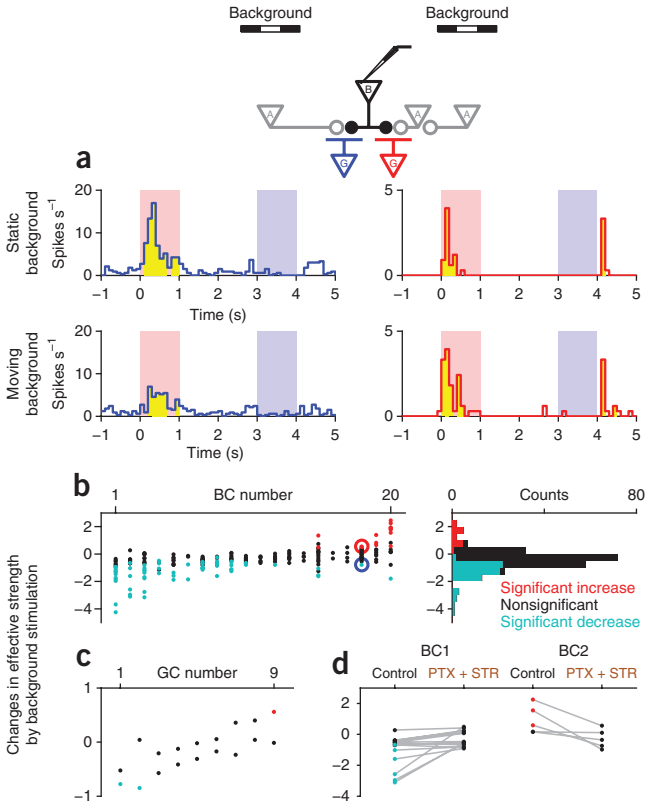

Figure 8 Amacrine cells can gate individual bipolar cell signals. (**a**) Response of two ganglion cells to bipolar cell stimulation alone (top) or in conjunction with visual stimulation in a distant annulus (bottom). The visual stimulus served to drive lateral amacrine cell circuits (see circuit diagram and Online Methods). Under these conditions, the response of one ganglion cell to the central bipolar cell was suppressed (left), whereas that of the other ganglion cell was enhanced (right). (**b**) Changes in effective strength of bipolar cell–ganglion cell connections elicited by distant visual stimulation (–0.47 ± 0.87, mean ± s.d. from 221 ganglion cells). Left, each dot represents one bipolar cell–ganglion cell connection (colored circles from **a**), and each column is one bipolar cell. 15 out of 20 bipolar cells showed distinct modulations among their connections. This variation from individual bipolar cell signals accounted for 59% of the total variation. Right, stacked histogram across all connections. Background stimulation weakened 65 connections (cyan; see left side of the circuit diagram at top), but strengthened 15 connections (red; right side). (**c**) The effects of background stimulation on convergent connections from two different bipolar cells. Data are presented as in **b**, but columns correspond to individual ganglion cells. In three of nine cases, the two bipolar cell–ganglion cell connections experienced significantly different gating (see **Supplementary Fig. 4** for an example). (**d**) The effects of background visual stimulation on the transmission from central bipolar cells to ganglion cells before (left) and after (right) applying inhibitory transmission blockers. The drug application eliminated both the suppressive and facilitatory gating effects ($P < 0.007$, χ^2 test; $P < 0.02$, Levene's test; see **Supplementary Fig. 5** for an example).

the visual field, and multiple amacrine cells at different locations are involved in modulating bipolar cell–ganglion cell connections[14,19,40]. To explore the details of this modulation, we proceeded to drive the amacrine cell circuits independently by a visual stimulus while monitoring their effect on transmission from individual bipolar cells.

Specifically, we projected on the retina a randomly moving grating, but excluded the receptive field center of the target bipolar cell and ganglion cells (see Online Methods). The stimulus by itself did not affect the baseline activity of the ganglion cells (**Fig. 8a** and **Supplementary Figs. 4b** and **5**), indicating that they did not receive any excitatory inputs directly from the light-driven bipolar cells, and we selected these ganglion cells for subsequent analysis. In contrast, this visual stimulus drives neurons in the periphery, including polyaxonal amacrine cells whose processes are long enough to interact with the selected bipolar cell and ganglion cells[17,24,40]. By combining such visual stimulation and single bipolar cell current injection, we were able to examine how light-driven amacrine cells modify the ganglion cell responses to the current-driven bipolar cells.

The background visual stimulation had diverse effects on bipolar cell–ganglion cell transmission. The response to bipolar cell depolarization was suppressed for some ganglion cells (**Fig. 8a**), enhanced for others (**Fig. 8a**) and unaffected for the rest (**Fig. 8b**). We observed effects of opposite sign even for transmission from the same bipolar cell (**Fig. 8a**,**b**). Of the total variation in these gating effects from distant stimuli, about 60% originated in diversity among connections from individual bipolar cells (**Fig. 8b**). Similarly, there was diversity among inputs converging onto a given ganglion cell; the same ganglion cell could experience suppression for one bipolar cell input, but not for another (**Fig. 8c** and **Supplementary Fig. 4b**).

A block of inhibitory transmission from amacrine cells eliminated these effects of peripheral visual stimulation (**Fig. 8d** and **Supplementary Fig. 5**). This indicates that amacrine cells mediate both the observed suppression and enhancement of bipolar cell transmission, the latter presumably through disinhibition via serial amacrine cell connections[41]. We conclude that the gating of bipolar cell signals by distant stimuli occurs independently at each bipolar cell–ganglion cell connection and that amacrine cells innervate these synapses in a way that allows the selective switching of each connection.

DISCUSSION

To examine how bipolar cell signals feed into ganglion cells, we simultaneously recorded from many ganglion cells while manipulating individual bipolar cells intracellularly, associated amacrine cells pharmacologically and surrounding circuits visually (**Fig. 1**). We found considerable divergence and convergence of diverse excitatory signals from bipolar cells to ganglion cells, indicating that individual bipolar cell–ganglion cell connections have distinct transfer functions despite their close proximity. First, a single bipolar cell was able to elicit sustained responses in some ganglion cells and sharply transient responses in others (**Fig. 2**). Such diverse kinetics of signal transmission resulted largely from inhibitory circuits involving amacrine cells (**Figs. 3** and **4**). Second, distinct modes of adaptation were found in transmission from individual bipolar cells, as indicated by slow changes of the response amplitude and latency over time (**Figs. 5** and **6**). Again, this diversity was shaped by amacrine cell circuits. Third, the synapses of the same bipolar cell differed considerably in their degree of rectification. This feature appeared to be intrinsic to a given bipolar cell–ganglion cell connection without the contribution of amacrine cell circuits (**Fig. 7** and **Supplementary Fig. 3**). Finally, bipolar cell–ganglion cell connections were individually modulated by amacrine cells; some were suppressed and others were enhanced (**Fig. 8** and **Supplementary Figs. 4** and **5**). Taken together, our results emphasize the diverse modes of bipolar cell–ganglion cell transmission and how it may be tuned by amacrine cells.

Putative mechanisms for diversity of bipolar cell synapses

What are the synaptic mechanisms for this diversity among the signals from a single bipolar cell? At this point we can only speculate,

but there are some plausible candidates. In most bipolar cells, across many species, the axon branches in a tree with many synaptic terminals near the tips[3,6,17,25,26] (**Fig. 1b**). Furthermore, amacrine cells contact the bipolar cell specifically at its terminals, often in direct proximity to the glutamate release sites[11,42]. Thus, it is tempting to identify the bipolar cell terminal as the key compartment that controls the bipolar cell–ganglion cell connection. This requires that different terminals be sufficiently isolated electrically or with respect to their calcium signals. Even in a terminal, there is evidence of presynaptic specializations that might differentially control transmission to different postsynaptic partners[43]. Alternatively, the key compartment may lie in the ganglion cell dendrite, with the transmission characteristics determined by the postsynaptic complement of transmitter receptors, local membrane dynamics and amacrine cell innervation. Again, this would require that different parts of the ganglion cell dendrite operate independently, although there is some evidence that salamander ganglion cells are electrotonically compact[44]. Clearly, one would like to directly observe the activity in presynaptic terminal arbors and postsynaptic dendritic trees, and new methods of targeted optical imaging may make this possible in the near future[45]. Here we consider in more detail possible mechanisms for our specific observations.

Regarding the diversity in transmission kinetics (**Figs. 2** and **3**), two factors mentioned above are known to affect the time course of the ganglion cell response: presynaptic depletion of vesicles makes for a transient postsynaptic response[20,21,32], and feedback or feedforward inhibition from amacrine cells can truncate the postsynaptic response[11–13]. Notably, these two mechanisms would react in opposite ways to the block of amacrine cell activity. The removal of tonic presynaptic inhibition would enhance transmitter release and speed depletion, thereby further shortening the response. In contrast, removal of feedback or feedforward inhibition would extend the response. Simulations of bipolar cell–ganglion cell transmission showed that a combination of synaptic depression and inhibition would indeed be sufficient to produce the observed bidirectional changes in the transmission dynamics (**Fig. 4**).

Certain forms of contrast adaptation in the retina have been traced to a reduction of transmitter release from bipolar cells[22–24]. This might be explained again by a process of presynaptic depletion[20,21]. Normally, the bipolar cell terminal receives tonic inhibition from amacrine cells[31], which lowers the synaptic release and therefore counteracts depletion. When inhibition was blocked, the depletion effects became more pronounced, which may explain why most bipolar cell–ganglion cell synapses became desensitizing (**Fig. 5g**). Alternatively, the increase in ganglion cell firing may modulate the behavior of postsynaptic conductances. This could contribute to contrast adaptation of individual connections[33,34], as long as their dendritic compartments are electrotonically separated.

Rectification is a well-known aspect of vesicle release at all synapses. However, the ribbon synapses at bipolar cell terminals are somewhat special; they allow for tonic release of glutamate and a continuous modulation of the release rate[46]. The rate increases nonlinearly with presynaptic voltage, owing largely to the voltage-dependent calcium influx[38,39]. The degree of rectification then depends on the bipolar cell resting potential and the voltage range during neural signaling. If the resting potential is high and the range is small, the modulation of the release rate may be essentially linear about the resting rate (**Supplementary Fig. 3**). In our experiments, the presynaptic voltage drive was deliberately large, and most bipolar cell–ganglion cell connections therefore showed asymmetric effects of depolarization and hyperpolarization. Nevertheless, different synapses were clearly operating along different parts of the voltage-release curve (**Fig. 7**).

Finally, the gating of bipolar cell–ganglion cell transmission by distant visual stimuli (**Fig. 8** and **Supplementary Figs. 4** and **5**) could be accomplished by presynaptic inhibition from polyaxonal amacrine cells[17,24,40,47]. Indeed, these stimuli hyperpolarized the bipolar cell soma[17] (**Supplementary Fig. 4a**). Given that some connections from the same bipolar cell were unaffected (**Fig. 8**), this view requires that certain terminals receive the inhibition and others not; the hyperpolarization at the soma then reflects an average over these inputs. The morphology of polyaxonal amacrine cells makes such a selective connectivity plausible: they carry sparse, straight and unbranched axons[17,40,48]. As such an axon passes through a bipolar cell terminal arbor, it can contact only a few of the terminals that lie in its path. Thus, different terminals will be innervated by different polyaxonal amacrine cells, allowing for the observed diversity in gating.

Implications for retinal computation

In a simple view of neural circuits, the nerve cells are treated as the active components, with fibers and synapses merely conducting signals between them. From our data, we conclude that each connection between neurons in the inner plexiform layer is an active circuit element whose transmission parameters are drawn from a broad palette of component options and whose performance is controlled by its own microcircuit (**Supplementary Fig. 6**). These individual bipolar cell–ganglion cell connections may be the primitives of retinal computation, much as transistors form the primitives for an electronic computer.

What are the potential benefits for retinal functions of such a fine-grained control of visual signals? First, this organization permits a greater range of distinct visual computations to proceed in parallel. For an illustration of this principle beyond our results, consider the ON-OFF direction-selective ganglion cells (DSGCs). These neurons fire selectively when a spot moves in one direction, but not when it moves in the opposite direction[19]. They are sensitive to tiny motions in the receptive field[49], and the fundamental computation therefore happens locally, in part from presynaptic inhibition of a bipolar cell terminal by a starburst amacrine cell (SAC) dendrite. The bipolar cell itself is not direction selective, but the SAC dendrite is; thus, the bipolar cell terminal becomes a direction-selective feature detector. Our observations (**Supplementary Fig. 1**) suggest that each bipolar cell contributes its terminals to DSGCs with all four directional preferences, by combining with different SAC dendrites. If each bipolar cell instead had just one type of synaptic output, then each DSGC would receive input from only a quarter of the bipolar cells. By exploiting individual bipolar cell–ganglion cell connections as elementary feature detectors, the retina uses its limited resources efficiently.

Second, the independent control of the various bipolar cell–ganglion cell connections shapes the way the retina adapts to prolonged visual stimulation. Among all of the bipolar cell inputs feeding a ganglion cell, any given visual stimulus will drive only a subset strongly. These connections will adapt, for example, owing to the synaptic depletion discussed above, and the sensitivity of the ganglion cell to that prolonged stimulus gradually declines. Meanwhile, the cell retains high sensitivity to novel stimuli that drive the previously dormant bipolar cell inputs. For example, a ganglion cell may desensitize to persistent stimuli with a certain orientation while retaining high sensitivity to novel stimuli of the orthogonal orientation[50]. In general, this organization allows the retina to implement a pattern-selective adaptation that has long been thought to arise only in higher visual areas[14].

Finally, the gain of a given bipolar cell–ganglion cell connection is not only a function of its recent activity, but can be controlled by

presynaptic amacrine cell circuits (**Fig. 8**). When this modulation affects different synapses in opposite directions, the selectivity of the receiving ganglion cell may be altered markedly. For example, for some ganglion cells, the polarity of the light response can switch from OFF type to ON type, depending on the activity in distant amacrine cells[40]. This suggests a flexible routing of signals from different bipolar cell pathways into one ganglion cell, and similarly from the same bipolar cell to different ganglion cells (**Fig. 8**). Such fine-scale routing is an essential feature of artificial computing machines, and its full implications for neuronal circuits remain to be explored.

METHODS

Methods and any associated references are available in the online version of the paper.

Note: Supplementary information is available in the online version of the paper.

ACKNOWLEDGMENTS

We gratefully acknowledge E. Soucy for his extensive help with the experiments, as well as all of the members of the Meister laboratory for many useful discussions. This work was supported by a Postdoctoral Fellowship for Research Abroad from the Japan Society for the Promotion of Science (H.A.) and grants from the US National Institutes of Health (M.M.).

AUTHOR CONTRIBUTIONS

H.A. and M.M. designed the study and wrote the manuscript. H.A. performed the experiments and analysis.

COMPETING FINANCIAL INTERESTS

The authors declare no competing financial interests.

Published online at http://www.nature.com/doifinder/10.1038/nn.3241.
Reprints and permissions information is available online at http://www.nature.com/reprints/index.html.

1. Wässle, H. Parallel processing in the mammalian retina. *Nat. Rev. Neurosci.* **5**, 747–757 (2004).
2. Masland, R.H. The fundamental plan of the retina. *Nat. Neurosci.* **4**, 877–886 (2001).
3. Wu, S.M., Gao, F. & Maple, B.R. Functional architecture of synapses in the inner retina: segregation of visual signals by stratification of bipolar cell axon terminals. *J. Neurosci.* **20**, 4462–4470 (2000).
4. Ghosh, K.K., Bujan, S., Haverkamp, S., Feigenspan, A. & Wässle, H. Types of bipolar cells in the mouse retina. *J. Comp. Neurol.* **469**, 70–82 (2004).
5. Roska, B., Molnar, A. & Werblin, F.S. Parallel processing in retinal ganglion cells: how integration of space-time patterns of excitation and inhibition form the spiking output. *J. Neurophysiol.* **95**, 3810–3822 (2006).
6. Boycott, B.B. & Wässle, H. Morphological classification of bipolar cells of the primate retina. *Eur. J. Neurosci.* **3**, 1069–1088 (1991).
7. Awatramani, G.B. & Slaughter, M.M. Origin of transient and sustained responses in ganglion cells of the retina. *J. Neurosci.* **20**, 7087–7095 (2000).
8. Mariani, A.P. Bipolar cells in monkey retina selective for the cones likely to be blue-sensitive. *Nature* **308**, 184–186 (1984).
9. Slaughter, M.M. & Miller, R.F. 2-amino-4-phosphonobutyric acid: a new pharmacological tool for retina research. *Science* **211**, 182–185 (1981).
10. DeVries, S.H. Bipolar cells use kainate and AMPA receptors to filter visual information into separate channels. *Neuron* **28**, 847–856 (2000).
11. Tachibana, M. & Kaneko, A. Retinal bipolar cells receive negative feedback input from GABAergic amacrine cells. *Vis. Neurosci.* **1**, 297–305 (1988).
12. Nirenberg, S. & Meister, M. The light response of retinal ganglion cells is truncated by a displaced amacrine circuit. *Neuron* **18**, 637–650 (1997).
13. Dong, C.J. & Werblin, F.S. Temporal contrast enhancement via $GABA_C$ feedback at bipolar terminals in the tiger salamander retina. *J. Neurophysiol.* **79**, 2171–2180 (1998).
14. Gollisch, T. & Meister, M. Eye smarter than scientists believed: neural computations in circuits of the retina. *Neuron* **65**, 150–164 (2010).
15. Enroth-Cugell, C. & Freeman, A.W. The receptive-field spatial structure of cat retinal Y cells. *J. Physiol. (Lond.)* **384**, 49–79 (1987).
16. Demb, J.B., Zaghloul, K., Haarsma, L. & Sterling, P. Bipolar cells contribute to nonlinear spatial summation in the brisk-transient (Y) ganglion cell in mammalian retina. *J. Neurosci.* **21**, 7447–7454 (2001).
17. Baccus, S.A., Ölveczky, B.P., Manu, M. & Meister, M. A retinal circuit that computes object motion. *J. Neurosci.* **28**, 6807–6817 (2008).
18. Enroth-Cugell, C. & Robson, J.G. The contrast sensitivity of retinal ganglion cells of the cat. *J. Physiol. (Lond.)* **187**, 517–552 (1966).
19. Demb, J.B. Cellular mechanisms for direction selectivity in the retina. *Neuron* **55**, 179–186 (2007).
20. Burrone, J. & Lagnado, L. Synaptic depression and the kinetics of exocytosis in retinal bipolar cells. *J. Neurosci.* **20**, 568–578 (2000).
21. Singer, J.H. & Diamond, J.S. Vesicle depletion and synaptic depression at a mammalian ribbon synapse. *J. Neurophysiol.* **95**, 3191–3198 (2006).
22. Jarsky, T. *et al.* A synaptic mechanism for retinal adaptation to luminance and contrast. *J. Neurosci.* **31**, 11003–11015 (2011).
23. Oesch, N.W. & Diamond, J.S. Ribbon synapses compute temporal contrast and encode luminance in retinal rod bipolar cells. *Nat. Neurosci.* **14**, 1555–1561 (2011).
24. Ölveczky, B.P., Baccus, S.A. & Meister, M. Retinal adaptation to object motion. *Neuron* **56**, 689–700 (2007).
25. Wässle, H., Puller, C., Müller, F. & Haverkamp, S. Cone contacts, mosaics and territories of bipolar cells in the mouse retina. *J. Neurosci.* **29**, 106–117 (2009).
26. Zhang, A.-J. & Wu, S.M. Receptive fields of retinal bipolar cells are mediated by heterogeneous synaptic circuitry. *J. Neurosci.* **29**, 789–797 (2009).
27. Zhang, A.-J. & Wu, S.M. Responses and receptive fields of amacrine cells and ganglion cells in the salamander retina. *Vision Res.* **50**, 614–622 (2010).
28. Arai, I., Tanaka, M. & Tachibana, M. Active roles of electrically coupled bipolar cell network in the adult retina. *J. Neurosci.* **30**, 9260–9270 (2010).
29. Mittman, S., Taylor, W.R. & Copenhagen, D.R. Concomitant activation of two types of glutamate receptor mediates excitation of salamander retinal ganglion cells. *J. Physiol. (Lond.)* **428**, 175–197 (1990).
30. Lukasiewicz, P.D., Lawrence, J.E. & Valentino, T.L. Desensitizing glutamate receptors shape excitatory synaptic inputs to tiger salamander retinal ganglion cells. *J. Neurosci.* **15**, 6189–6199 (1995).
31. Jones, S.M. & Palmer, M.J. Activation of the tonic $GABA_C$ receptor current in retinal bipolar cell terminals by nonvesicular GABA release. *J. Neurophysiol.* **102**, 691–699 (2009).
32. von Gersdorff, H. & Matthews, G. Depletion and replenishment of vesicle pools at a ribbontype synaptic terminal. *J. Neurosci.* **17**, 1919–1927 (1997).
33. Kim, K.J. & Rieke, F. Temporal contrast adaptation in the input and output signals of salamander retinal ganglion cells. *J. Neurosci.* **21**, 287–299 (2001).
34. Kim, K.J. & Rieke, F. Slow Na^+ inactivation and variance adaptation in salamander retinal ganglion cells. *J. Neurosci.* **23**, 1506–1516 (2003).
35. Kastner, D.B. & Baccus, S.A. Coordinated dynamic encoding in the retina using opposing forms of plasticity. *Nat. Neurosci.* **14**, 1317–1322 (2011).
36. Rieke, F. Temporal contrast adaptation in salamander bipolar cells. *J. Neurosci.* **21**, 9445–9454 (2001).
37. Baccus, S.A. & Meister, M. Fast and slow contrast adaptation in retinal circuitry. *Neuron* **36**, 909–919 (2002).
38. Heidelberger, R., Heinemann, C., Neher, E. & Matthews, G. Calcium dependence of the rate of exocytosis in a synaptic terminal. *Nature* **371**, 513–515 (1994).
39. Matsui, K., Hosoi, N. & Tachibana, M. Excitatory synaptic transmission in the inner retina: paired recordings of bipolar cells and neurons of the ganglion cell layer. *J. Neurosci.* **18**, 4500–4510 (1998).
40. Geffen, M.N., de Vries, S.E.J. & Meister, M. Retinal ganglion cells can rapidly change polarity from Off to On. *PLoS Biol.* **5**, e65 (2007).
41. Roska, B., Nemeth, E. & Werblin, F.S. Response to change is facilitated by a three-neuron disinhibitory pathway in the tiger salamander retina. *J. Neurosci.* **18**, 3451–3459 (1998).
42. Dowling, J.E. & Werblin, F.S. Synaptic organization of the vertebrate retina. *Virus Res.* **11**, 1–15 (1971).
43. Brandstätter, J.H., Koulen, P., Kuhn, R., van der Putten, H. & Wässle, H. Compartmental localization of a metabotropic glutamate receptor (mGluR7): two different active sites at a retinal synapse. *J. Neurosci.* **16**, 4749–4756 (1996).
44. Taylor, W.R., Mittman, S. & Copenhagen, D.R. Passive electrical cable properties and synaptic excitation of tiger salamander retinal ganglion cells. *Vis. Neurosci.* **13**, 979–990 (1996).
45. Dreosti, E., Esposti, F., Baden, T. & Lagnado, L. *In vivo* evidence that retinal bipolar cells generate spikes modulated by light. *Nat. Neurosci.* **14**, 951–952 (2011).
46. Lagnado, L., Gomis, A. & Job, C. Continuous vesicle cycling in the synaptic terminal of retinal bipolar cells. *Neuron* **17**, 957–967 (1996).
47. Cook, P.B. & McReynolds, J.S. Lateral inhibition in the inner retina is important for spatial tuning of ganglion cells. *Nat. Neurosci.* **1**, 714–719 (1998).
48. Famiglietti, E.V. Polyaxonal amacrine cells of rabbit retina: morphology and stratification of PA1 cells. *J. Comp. Neurol.* **316**, 391–405 (1992).
49. Barlow, H.B. & Levick, W.R. The mechanism of directionally selective units in rabbit's retina. *J. Physiol. (Lond.)* **178**, 477–504 (1965).
50. Hosoya, T., Baccus, S.A. & Meister, M. Dynamic predictive coding by the retina. *Nature* **436**, 71–77 (2005).

ONLINE METHODS

Electrophysiology. Simultaneous intracellular and multielectrode recording was performed as described previously[17], following protocols approved by the Institutional Animal Care and Use Committee at Harvard University. In short, the dark-adapted retina of a tiger salamander (*Ambystoma tigrinum*, both sexes, age unspecified, but in the larval stage) was isolated and placed on a flat array of 61 extracellular electrodes with the ganglion cell side down (**Fig. 1a**). The retina was superfused with oxygenated Ringer's medium (110 mM NaCl, 22 mM $NaHCO_3$, 2.5 mM KCl, 1.6 mM $MgCl_2$, 1 mM $CaCl_2$ and 10 mM D-glucose, equilibrated with 95% O_2 and 5% CO_2 gas) at ~25 °C. Sharp intracellular microelectrodes were filled with 2 M potassium acetate and 3% rhodamine dextran 10,000 MW (wt/vol, fluorescent dye, Molecular Probes) with a final impedance of 150–250 MΩ, and blindly inserted into various cells until one with visual response characteristics matching those of bipolar cells was found[37]. We sampled the signals from each extra- and intracellular electrode at 10 kHz, and used an Axoclamp 2B amplifier (Molecular Devices) in bridge mode for intracellular recordings and current injection into bipolar cells. In all experiments, we alternately delivered depolarizing and hyperpolarizing square pulse currents (500 pA, 1 s each) into bipolar cells with 2-s intervals (**Fig. 1d**). Each trial of this protocol therefore lasted for 6 s, and each bipolar cell was typically examined with 30–100 trials. In some experiments, we also used a train of square-wave pulse currents (±500 pA, 1 Hz, 10 s) to deplete transmission from the intracellularly stimulated bipolar cell (10–15 trials with 10-s intervals; **Fig. 6c–e**).

Visual stimulation. Visual stimuli were displayed on a gamma-corrected cathode-ray tube monitor (DELL E773c, frame rate = 100 Hz, mean luminance = ~18 mW m^{-2}) and projected on the photoreceptor layer of the retina as described previously[17]. Bipolar cells were identified during the experiment by their responses to center spot (~200-μm diameter), annulus ring (~500-μm inner diameter, ~1,000-μm outer diameter) and full-field flash stimuli. The spatio-temporal receptive fields of bipolar cells and ganglion cells were mapped using flickering checkerboard stimuli[51] for 10–15 min, with square fields 20–100 μm in width, each modulated independently by white noise (**Supplementary Fig. 1**).

To characterize how ganglion cell responses adapt to bipolar cell inputs (**Fig. 6c–e**), we stimulated the ganglion cells in two ways: by single bipolar cell current injection to induce adaptation in one bipolar cell pathway, and by visual stimulation to probe the effects on other bipolar cell pathways. The visual stimulus was comprised of black and white stripes (80-μm width) confined to an annulus region (outer diameter, 1,000 μm; inner diameter, 500 μm; centered at the bipolar cell soma) and its contrast was inverted twice (with 0.5-s interval) 3 s before and immediately after repetitive intracellular stimulation of a single bipolar cell (see above). Note that this visual stimulus did not change its mean intensity, and it intersected with the receptive field center of the ganglion cell, but not that of the current-stimulated bipolar cell.

To examine how amacrine cells gate the synaptic transmission between bipolar cells and ganglion cells (**Fig. 8** and **Supplementary Figs. 4** and **5**), the entire visual field (6,400 × 4,800 μm) was covered by a grating of black and white stripes (80-μm width) and divided into a circular center region (1,000 μm in diameter, centered at the bipolar cell soma) and the surrounding background region[17,24]. In combination with the current injection into a bipolar cell, the surrounding grating was then either shifted by a half period every 200 ms or jittered on every 10-ms frame update (Gaussian random motion with a s.d. of 2 mm s^{-1}, corresponding to a step size of 2 pixels per frame) to recruit inputs from polyaxonal amacrine cells[17,40]. The center region remained static so as not to visually stimulate the current-stimulated bipolar cell or ganglion cells nearby. In the former shifting case, every current injection trial was delayed by 50 ms in order to vary the relative timing between the onset of square pulse currents and that of background stimulus motion. We also inverted the contrast of the center and surrounding gratings in or out of phase to examine the bipolar cell response characteristics[17] (**Supplementary Fig. 4a**).

Data analysis. For extracellular recordings, spike trains from individual ganglion cells were extracted from raw voltage traces by a semi-automated spike-sorting algorithm written in Igor (Wave Metrics). In total we identified 4,236 ganglion cells (mean spontaneous firing rate, 1.0 Hz; s.d., 2.2 Hz; median, 0.20 Hz), of which 965 ganglion cells showed significant responses to single bipolar cell stimulation and were used for subsequent analyses. Note that the ganglion cell layer also contains some displaced amacrine cells, but their action potentials are expected to be below the noise level of the multielectrode recordings and are attenuated further by signal filtering before spike sorting[52]. The extracted spike timing data and intracellular data traces were then analyzed in Matlab (MathWorks). Significance level is 0.05 in all analyses.

Receptive field analysis. The spatio-temporal receptive fields of bipolar cells and ganglion cells were estimated by reverse-correlation methods[17,51]. Using the random flicker stimulus, we computed the response-weighted average of the stimulus waveform, where the weight is the measured membrane voltage for bipolar cells (**Supplementary Fig. 1a**), and spike number for ganglion cells (**Supplementary Fig. 1b–e**). To display the receptive field locations, we computed two-dimensional Gaussian fits to the spatial receptive field and assigned the cell's location to the center of that profile (**Fig. 1c**).

Effective connection strength. To quantify transmission from bipolar cells to ganglion cells, we first computed the PSTH (0.1-s bin width) of ganglion cell spiking activity while manipulating bipolar cell activity intracellularly. For those ganglion cells that had significantly different firing rates from their spontaneous activity (r_{spont}; based on the activity 1 s before the onset of current injection) in at least one bin during the current injection periods (two-tailed with Bonferroni correction), we calculated the average firing rates for the 1-s periods of bipolar cell depolarization and hyperpolarization (r_{dep} and r_{hyp}, respectively). If the difference ($r_{dep} - r_{hyp}$) was significantly above or below zero, then we considered that the bipolar cell had sign-preserving or sign-inverting effects on the ganglion cell activity, respectively. The confidence interval was estimated by bootstrap resampling methods over trials (10,000 repeats). The effective strength of the bipolar cell–ganglion cell connection was then defined as

$$\mathrm{ES[dep;hyp]} = \frac{r_{dep} - r_{hyp}}{\sqrt{\frac{s_{dep}^2 + s_{hyp}^2}{2}}} \quad (1)$$

where s_{dep} and s_{hyp} are the s.d. of the ganglion cell firing rates across trials on bipolar cell depolarization and hyperpolarization, respectively.

This standardized measure (called the effect size in statistics) does not depend on the data length (number of trials), unlike the *P* values in the significance tests. Changes in ES[dep;hyp] were used as a measure of the effects of background visual stimulation on bipolar cell–ganglion cell connections (**Fig. 8b–d**). Estimation of statistical significance followed the confidence intervals of ES[dep;hyp] in the presence and absence of the background stimulation. The Levene's test (for the equality of variance) and χ^2 test (for the independence of the observed frequencies of the significant changes in ES[dep;hyp]) were used to judge the effects of the drug application across the population (**Fig. 8d**).

Diversity of signals from individual bipolar cells. To quantify the divergence of bipolar cell signals, we partitioned the total variation of ganglion cell response characteristics into the sum of the variation among inputs from individual bipolar cells and the variation across different bipolar cells, much as in the analysis of variance. Formally,

$$\sum_{i,j}\left(x_{ij} - x_{..}\right)^2 = \sum_{i,j}\left(x_{ij} - x_{i.}\right)^2 + \sum_{i,j}\left(x_{i.} - x_{..}\right)^2 \quad (2)$$

$$\text{Total variation} = \text{Variation among BCs} + \text{Variation across BCs}$$

where x_{ij} is any given response property of interest for j^{th} ganglion cell in response to i^{th} bipolar cell (BC) stimulation (for $i = 1, \ldots, n$ and $j = 1, \ldots, m_i$), and $x_{i.}$ and $x_{..}$ indicate the average over j and over all cell pairs, respectively. The fraction of the total variation that results from variation among inputs from individual bipolar cells was then computed from equation (2).

Dynamics. To analyze the dynamics of bipolar cell–ganglion cell connectivity, we fit the PSTHs of ganglion cells in response to bipolar cell depolarization with the unimodal function $f(t) = \alpha t^{\beta} \exp(-t/\gamma) + r_{spont}$, where α, β and γ denote the free parameters, t (>0) indicates the time after the onset of current injection, and

doi:10.1038/nn.3241

r_{spont} is the spontaneous firing rate. The peak latency was then computed as $t_{peak} = \beta\gamma$ and the peak firing rate as $r_{peak} = f(t_{peak}) - r_{spont}$. Confidence intervals on the fit parameters were used for judging whether significant variation existed among different bipolar cell–ganglion cell connections (**Fig. 2c**,**d**). The sign test was used to examine the changes in r_{peak} before and after drug application (**Fig. 3c**), and the Levene's test was used to assess the changes in the distribution of t_{peak} (**Fig. 3d**).

Adaptation. For those ganglion cells with low spontaneous firing rates ($r_{spont} \leq$ 1 Hz), but high peak rates ($r_{peak} \geq 5$ Hz), we analyzed the variation of the peak rate and latency across trials to examine adaptive changes in bipolar cell–ganglion cell transmission over time (**Figs. 5** and **6**). We first computed the peak rate and latency using a moving window of ten trials, and performed a linear regression over trials. We then considered that the peak rate showed desensitization or sensitization if the slope was significantly below or above zero, respectively. For the peak latency, significant decrease or increase over trials indicates sensitization or desensitization, respectively. Note that the rate adaptation did not necessarily coincide with the latency adaptation (**Fig. 5c**,**d**). These slope values were used for the divergence analysis (**Fig. 5e**), and the χ^2 test was used for examining the effects of the inhibitory transmission blockers (**Fig. 5g**).

To address whether the adaptation arises before or after ganglion cells integrate their synaptic inputs from bipolar cells (**Fig. 6**), we examined whether adaptation in one bipolar cell pathway (driven by single bipolar cell current injection) affects the ganglion cell responses to inputs from other bipolar cell pathways (driven by a visual stimulus). A single exponential function was used to fit the time course of ganglion cell responses to repetitive intracellular stimulation of single bipolar cells (**Fig. 6c**,**d**). The sign test was used to compare the ganglion cell visual responses before and after the adaptation by the current injection (r_{before} and r_{after}, respectively, using the spike counts during the 1-s visual stimulation periods; **Fig. 6e**).

Rectification. For those ganglion cells with sufficiently high spontaneous firing rates ($r_{spont} \geq 1$ Hz), we investigated if the bipolar cell–ganglion cell synaptic transmission was rectified or not (**Fig. 7**). Specifically, we used bootstrap resampling methods over trials (10,000 repeats) to analyze the differences of r_{dep} and r_{hyp} from r_{spont}. We considered that the synaptic transmission was rectified if either r_{dep} or r_{hyp} was significantly different from r_{spont}, and nonrectified if both r_{dep} and r_{hyp} were significantly different from r_{spont}. The rectification index was defined as

$$\frac{\mathrm{ES[dep;spont]} - \mathrm{ES[spont;hyp]}}{\mathrm{ES[dep;spont]} + \mathrm{ES[spont;hyp]}} \quad (3)$$

where ES[dep;spont] and ES[spont;hyp] from equation (1) indicate the effective strength of bipolar cell depolarization and hyperpolarization, respectively (**Fig. 7b**,**d**). Note that ES[dep;spont] >0 for an increase in ganglion cell spiking activity on bipolar cell depolarization, whereas ES[spont;hyp] >0 for a decrease in ganglion cell spiking activity on bipolar cell hyperpolarization. The index is therefore close to unity for rectifying excitatory transmission because ES[dep;spont] >0 and ES[spont;hyp] ≈ 0, whereas the index is near zero for nonrectifying transmission because ES[dep;spont] ≈ ES[spont;hyp]. The rank-sum test (for the equality of median rectification indices) and the χ^2 test (for the independence of the observed frequencies of rectifying and nonrectifying bipolar cell–ganglion cell connections) were used to judge the effects of blocking inhibitory amacrine cell circuits (**Fig. 7d**).

Simulation. To examine the contributions of different amacrine cell circuits to the transmission dynamics from bipolar cells to ganglion cells (**Fig. 3**), we incorporated the following four types of amacrine cell inputs into a phenomenological model of the synaptic transmission[53] (**Fig. 4** and **Supplementary Fig. 7**); tonic presynaptic inhibition ($\alpha_{pre} > 0$), tonic postsynaptic inhibition ($\alpha_{post} > 0$), feedback presynaptic inhibition ($\beta_{pre} > 0$) and feedforward postsynaptic inhibition ($\beta_{post} > 0$). Specifically, the presynaptic side was modeled by the dynamics of the vesicle pool $x \in [0,1]$ and release factor $u \in [0,1]$

$$\frac{dx}{dt} = \frac{1-x}{\tau_d} - v \quad (4)$$

$$\frac{du}{dt} = \frac{u_0 - u}{\tau_f} + k(1-u)V_m \quad (5)$$

where τ_d and τ_f are the recovery constants of depression and facilitation, respectively. The release factor u works as a driving force of vesicle release, reflecting, for example, presynaptic calcium level[20,32]; u_0 and k indicate the baseline and a constant, respectively. The effective presynaptic membrane potential $V_m = V(I) - \alpha_{pre} - B_{pre}$ changes on receiving input current I with current-voltage transform V. When $V_m > 0$, neurotransmitters are released by the rate $v = [uxV_m]_+$ as in equation (4), where $[\cdot]_+$ is a half-wave rectification function, and the release factor u increases as in equation (5). With time constant τ, the released vesicles v recruit feedback or feedforward inhibition, $dB_*/dt = -B_*/\tau + v\beta_*$, where $*$ is either pre or post, respectively. The postsynaptic dynamics were then simulated by the firing rate $r = [v - \theta]_+$, where v is now considered as effective membrane potential and $\theta = \theta_0 + \alpha_{post} + B_{post}$ is the effective spiking threshold with a baseline of θ_0. Note that ganglion cells in the salamander retina are thought to be electrotonically compact for excitatory input[44]; and that voltage-dependent processing in the dendrites contributes little to signal integration[33].

The simulation was done at time steps of 1 ms using the following parameter values. For simplicity, we ignored the nonlinear effects of current-voltage transform in bipolar cells[54] and assumed $V(I) = IR_{in} + V_0$ with an input resistance $R_{in} =$ 100 MΩ and a baseline potential $V_0 = 0$ mV. Consistent with our experimental protocol, we used $I = 500$ pA for $t \in [0,1]$ s, otherwise 0 A. Previous studies suggest that recovery from synaptic depression after a sustained depolarization is slow[32], whereas the calcium dynamics are relatively fast and facilitatory[55] and the time course of retinal inhibition is even faster[56]. Thus, we used $\tau_d = 5$ s, $\tau_f = 0.5$ s, $u_0 = 0.01$, $k = 0.01$ s^{-1} mV^{-1}, and $\tau = 0.1$ s. For the postsynaptic side, we set $\theta_0 =$ 0.8 mV so that the normalized firing rate r decays within ~0.5 s in the absence of inhibition (**Fig. 3**). For the inhibition parameters, we used $\alpha_{pre} \in [0,3]$ mV, $\alpha_{post} \in [0,0.18]$ mV, $\beta_{pre} \in [0,0.75]$ mV and $\beta_{post} \in [0,1.5]$ mV (normalized in **Fig. 4** for display purposes). A stronger inhibition led to no firing responses in the postsynaptic side. We obtained qualitatively similar results over many different sets of the parameters, confirming that the model is robust in accounting for the effects of amacrine cell circuitry.

To examine how the rectification arises (**Fig. 7**), we also simulated the transmitter release rate v at different baseline potentials V_0 (**Supplementary Fig. 3**). Specifically, we used $V_0 = 0$, 7.5 and 15 mV with the injected current I following the protocol of **Figure 1d**, and ran the simulation with the same parameter values as described above, but with no inhibition ($\alpha_{pre} = \alpha_{post} = \beta_{pre} = \beta_{post} = 0$ mV).

51. Meister, M., Pine, J. & Baylor, D.A. Multi-neuronal signals from the retina: acquisition and analysis. *J. Neurosci. Methods* **51**, 95–106 (1994).
52. Segev, R., Goodhouse, J., Puchalla, J. & Berry, M.J. Recording spikes from a large fraction of the ganglion cells in a retinal patch. *Nat. Neurosci.* **7**, 1154–1161 (2004).
53. Tsodyks, M., Pawelzik, K. & Markram, H. Neural networks with dynamic synapses. *Neural Comput.* **10**, 821–835 (1998).
54. Mao, B.Q., MacLeish, P.R. & Victor, J.D. The intrinsic dynamics of retinal bipolar cells isolated from tiger salamander. *Vis. Neurosci.* **15**, 425–438 (1998).
55. Kaneko, A., Pinto, L.H. & Tachibana, M. Transient calcium current of retinal bipolar cells of the mouse. *J. Physiol. (Lond.)* **410**, 613–629 (1989).
56. Eggers, E.D. & Lukasiewicz, P.D. Receptor and transmitter release properties set the time course of retinal inhibition. *J. Neurosci.* **26**, 9413–9425 (2006).

Divergence of visual channels in the inner retina

Hiroki Asari and Markus Meister

Supplementary Information

Supplementary Figure Legends

Supplementary Figure 1: Ganglion cells with distinct visual response characteristics receive inputs from the same bipolar cell.

(a) The spatio-temporal receptive field (STRF) of a bipolar cell (BC; red hue, On-polarity; blue hue, Off-polarity). For simplicity, the STRF is shown only for one spatial dimension at the receptive field center. The contour of the full spatial receptive field is shown in **Fig. 1c** (green). The spatial (right, dark green) and temporal (top, light green) profiles of this STRF are shown for cuts at the locations indicated by arrows in the corresponding colors.

(b–e) Responses of four ganglion cells (GCs; "G" in the circuit diagram) simultaneously recorded during current injection ($\pm$500 pA; **Fig. 1d**) into a single bipolar cell ("B"; from **a**). Raster graph (top right) and peri-stimulus time histogram (PSTH; bottom right) displayed as in **Fig. 2**. While a distant GC (**b**) did not show any changes in its firing rate upon BC stimulation, GCs in the vicinity (**c–e**) increased their spiking activity upon BC depolarization. These three GCs also appear in **Fig. 1** with corresponding colors. Two of them were direction selective (DS) but with opposite preferred directions (**d**, upward; **e**, downward), whereas the third was non-DS (**c**; see their STRFs on the left, displayed as in **a**). This shows that GCs with very different feature selectivity can derive input from the same BC.

Note that the mean potential change in BCs from the 500 pA current injection (38 ± 4 mV; mean $\pm$ standard error from 86 BCs with resting potential of -38 ± 1 mV) was larger than the maximal light-evoked responses of the BCs (10 ± 1 mV; the range of membrane potential fluctuations in response to full-field contrast-inverting stimulus at 1 Hz, averaged across 30-50 trials). However, the effective connection strength (see Eq.(1) in Methods) increased linearly with injected current amplitudes (from 100 pA to 500 pA in steps of 100 pA with a slope of 0.28 nA^{-1}; $R^2 = 0.94$ from 7 GCs in 1 experiment with pharmacological block of inhibition), indicating that BC signals are not saturated within this range of the stimulation. We thus used 500 pA in this study to maximize the number of GCs for which spiking responses could be evaluated.

We also performed four sets of control experiments to eliminate alternative explanations of the results. First, to test for nonspecific ephaptic stimulation of GCs, we injected current into the extracellular space of the inner nuclear layer and found that the 500 pA stimulation did not drive any GC (203 GCs in total from 5 retinas, tested at 3 electrode locations each with 30 trials). This eliminates the possibility of nonspecific GC activation by the current injection.

Nature Neuroscience: doi:10.1038/nn.3241

Second, because many of the observations rely on comparisons under two sequential conditions, we examined the stationarity of the measurements over time. Using the identical current injection protocol we stimulated the same BC twice, separated by ∼25 minutes, comparable to the measurement intervals before and after drug applications. For each BC-GC pair we analyzed changes in the connection parameters across the two measurements (26 GCs total from stimulation of 5 BCs). The evoked spike counts were not significantly different except for one GC, and there was no significant change in any of the other transmission characteristics (mean difference between the two measurements ± standard error across the population): peak evoked rate, -0.8 ± 0.5 spikes s^{-1} ($p>0.3$, sign-test; 26 GCs); peak latency, 0.0 ± 0.1 s ($p>0.5$, sign-test; 26 GCs); peak rate change over successive 6-s trials, -0.13 ± 0.05 spikes s^{-1} per trial ($p>0.2$, sign-test; $p>0.6$, χ^2-test; 13 GCs); peak latency change, 1.4 ± 1.7 ms per trial ($p>0.5$, sign-test; $p>0.18$, χ^2-test; 13 GCs); rectification index, 0.10 ± 0.12 ($p>0.3$, sign-test; $p>0.3$, χ^2-test; 10 GCs); effects of background stimulation on effective connection strength, 0.04 ± 0.15 ($p>0.8$, sign-test; $p>0.4$, χ^2-test; 16 GCs in response to 3 BCs). Thus the recordings were sufficiently stable over time to allow reliable comparison between sequential conditions.

Third, to test for deleterious effects of excessive current injection, we tested BC-GC transmission at half the size of the injected current in 6 experiments (5 control conditions; 1 with inhibition block). The weaker BC stimulation drove fewer GCs with smaller responses (35 GCs responded at 250 pA stimulation, compared to 67 GCs at 500 pA), but the transmission properties were not strongly dependent on the injected current amplitude. Specifically, the mean values standard deviation are listed as follows for the 250 and 500 pA stimulation, respectively: peak evoked rate, 6.1 ± 5.4 and 13.0 ± 11.9 spikes s^{-1} ($p<0.001$, sign-test; 35 GCs); peak latency, 0.28 ± 0.10 and 0.24 ± 0.08 s ($p>0.2$, sign-test; 35 GCs); peak rate change over trials, -0.11 ± 0.26 and -0.28 ± 0.22 spikes s^{-1} per trial ($p>0.1$, sign-test; 22 GCs); peak latency change over trials, 6.8 ± 12.7 and 5.2 ± 10.3 ms per trial ($p>0.5$, sign-test; 22 GCs); rectification index, 0.42 ± 0.28 and 0.48 ± 0.56 ($p>0.5$, sign-test; $p>0.5$, χ^2-test; 11 GCs); effects of background stimulation on effective connection strength, -0.11 ± 0.54 and -0.09 ± 0.49 ($p>0.6$, sign-test; $p>0.5$, χ^2-test; 15 GCs in response to 2 BCs). Therefore, the standard current stimulus of 500 pA does not appear to distort the measured synaptic transmission properties, even though it exceeds the magnitude of visually evoked synaptic currents (∼100 pA; Wu *et al.*, 2000, *J Neurosci* **20**, 4462–4470). Note also that the depolarization evoked by this current (38 ± 4 mV; see above) is well within the physiological range of the membrane potential, and stable recordings from BCs have been reported with much larger currents (Thoreson & Burkhardt, 2003, *Vis Neurosci* **20**, 19–28).

Finally, we examined possible contributions of lateral signal spread within the BC network. We attempted to block the electrical synapses between BCs with a gap junction blocker (100 μM meclofenamic acid; Zhang & Wu, 2009, *J Neurosci* **29**, 789–797; Arai *et al.*, 2010, *J Neurosci* **30**, 9260–9270). After the drug application, only 19 out of 75 GCs remained responsive to the intracellularly stimulated BCs (6 BCs in total). Importantly, though, their response characteristics did not change significantly except for the effective connective strength. Specifically, blocking electrical synapses decreased the peak evoked rate from 7.4 ± 5.5 to 3.1 ± 1.7 spikes s^{-1} (mean ± standard deviation; $p<0.005$; sign-test; 19 GCs), but did not affect the peak latency (0.27 ± 0.08 s, control; 0.31 ± 0.11, drug; $p>0.06$, sign-test; $p>0.16$, Levene's test for the equality of

Nature Neuroscience: doi:10.1038/nn.3241

variance; 19 GCs) or the adaptation properties over successive trials ($p>0.11$ for the peak latency change; $p>0.06$ for the peak rate change; χ^2-test on 12 GCs). We also found one example each of rectifying and nonrectifying connections to the same BC in the absence of electrical coupling (rectification index: 0.63 and 0.04, respectively). Electrical synapses thus contribute to the lateral spread of signal from a BC, but the dynamics and nonlinearity of the connection appear to be dominated by the chemical BC-GC synapse. We further reduced the effect of electrical coupling on the data set by restricting analysis to BC-GC connections at $\leq$0.35 mm distance, within direct reach of the processes from the two neurons.

Supplementary Figure 2: Circuits of opposite polarity diverge from single bipolar cells.

(a) Two ganglion cells are driven by current injection into a single bipolar cell (OFF-type). One ganglion cell (OFF-type) fired on depolarization of the bipolar cell (left, PSTH in blue), but the other ganglion cell (ON-type) fired on hyperpolarization of the same bipolar cell (right, PSTH in red).

(b) Response of a single ganglion cell to stimulation of two different bipolar cells in serial recordings. The ganglion cell (OFF-type) fired on depolarization of one bipolar cell (left, OFF-type) but on hyperpolarization of the other bipolar cell (right, ON-type). This reflects a "push-pull" circuit in the inner retina in which the ON and OFF pathways exert opposite influences on the same GC.

(c) The effect of inhibitory signals from amacrine cells on transmission between one bipolar cell and two ganglion cells. *Left*: One ganglion cell was excited by the bipolar cell depolarization but only after amacrine cell signals were blocked pharmacologically by 100 μM picrotoxin (PTX) and 1.0 μM strychnine (STR). The inhibition may be presynaptic or postsynaptic or both. *Right*: The other ganglion cell was excited by the bipolar cell hyperpolarization, but this connection disappeared when inhibitory synaptic transmission was blocked. Because washout of these drugs from a whole-mount preparation is exceedingly slow, we could not achieve full reversal of the drug effects within the available time of 30-60 minutes for the intracellular recordings. Thus we only compared measurements before and after drug application, with no analysis of the washout.

Supplementary Figure 3: Baseline release rate can control the rectification and rebound responses.

Simulation on neurotransmitter release dynamics at bipolar cell synaptic terminals in response to depolarizing and hyperpolarizing current injection (top trace in **a**; see Methods for details). If the terminal has no baseline release rate (**a**), its output is rectified because the release rate cannot decline on hyperpolarization. If the terminal does release neurotransmitter at baseline (**b,c**), the synapse can transmit both depolarizing and hyperpolarizing signals. Interestingly, rebound responses at the offset of hyperpolarization emerge only at a high baseline release rate (**c**) due to an increased recovery of the vesicle pool during hyperpolarization. Consistent with this prediction, we found rebound responses more frequently for non-rectifying transmission (12 out of 40 pairs of bipolar and ganglion cells; e.g., **Fig. 7**, black PSTHs) than for rectifying transmission (5 out of 84 pairs; e.g., **Fig. 7**, red PSTHs).

Nature Neuroscience: doi:10.1038/nn.3241

Supplementary Figure 4: Individual bipolar cell terminals are gated presynaptically.

(a) Somatic membrane potential fluctuations of two bipolar cells in response to center and background grating stimuli whose contrast was inverted in or out of phase at 0.5 Hz (top traces; see also top circuit diagram). As in these two examples, most bipolar cells became hyperpolarized at the soma when the background grating alone inverted its contrast (arrowheads, 28 out of 39 cells; see also **Fig. 8b**, left), indicating the presence of inhibitory inputs from polyaxonal wide-field amacrine cells to bipolar cells (Baccus *et al.*, 2008, *J Neurosci* **28**, 6807–6817).

(b) Response of a ganglion cell to stimulation of two different bipolar cells (from **a**), with (bottom) and without (top) visual stimulation in the distant background. Moving background stimuli fully suppressed the ganglion cell responses to depolarization of one bipolar cell (left), but not to the other bipolar cell (right) even though the bipolar cell itself was hyperpolarized by the background stimulation (**a**, right, arrowheads). Presumably this presynaptic hyperpolarization is caused by amacrine cell inputs to different terminals of the same bipolar cell, whereas the terminals contributing to the ganglion cell inspected here are spared (see the right side of the circuit diagram).

Supplementary Figure 5: Amacrine cells mediate the effects of background visual stimulation on bipolar cell signal transmission.

Responses of a ganglion cell to bipolar cell stimulation with (bottom) and without (top) background motion stimuli, before (left) and after (right) blocking inhibitory synaptic transmission by 100 μM picrotoxin (PTX) and 1.0 μM strychnine (STR). Under the control condition, the background stimulation suppressed the ganglion cell responses to bipolar cell depolarization (left) but not after the drug application (right).

Supplementary Figure 6: Connections between bipolar and ganglion cells form diverse components in the circuit of the retina.

Schematic diagram illustrating a circuit model of the inner retina suggested by the present study. Distinct visual channels arise at individual connections between bipolar and ganglion cells because each has different transmission properties, such as rectifying (blue) or nonrectifying (cyan), and forms a distinct microcircuit with specific amacrine cells at different locations, such as tonic presynaptic inhibition (orange) or feedback inhibition (green). Each of these components shapes the signal in its own way. Ganglion cells then pool over their outputs for further processing of visual information.

Supplementary Figure 7: Circuit diagram of simulated synaptic transmission from bipolar to ganglion cells.

The model simulates how a step change in the input current (I) to a bipolar cell (green rectangle; V_{m}, membrane potential; x, vesicle pool; u, release rate) is transduced into an evoked firing rate (r) of a ganglion cell (blue rectangle; θ, spike threshold). See Methods for details (v, released vesicle; k, τ_{f}, and τ_{d}, free parameters). Specifically we analyzed how the dynamics are affected by the following four types of inhibitory inputs from amacrine cells (black rectangles); tonic presynaptic inhibition ($\alpha_{\mathrm{pre}}>0$), tonic postsynaptic inhibition ($\alpha_{\mathrm{post}}>0$), feedback presynaptic inhibition (B_{pre} with free parameter $\beta_{\mathrm{pre}}>0$), and feedforward postsynaptic inhibition (B_{post} with free parameter $\beta_{\mathrm{post}}>0$). See also the diagram in **Fig. 4**.

Nature Neuroscience: doi:10.1038/nn.3241

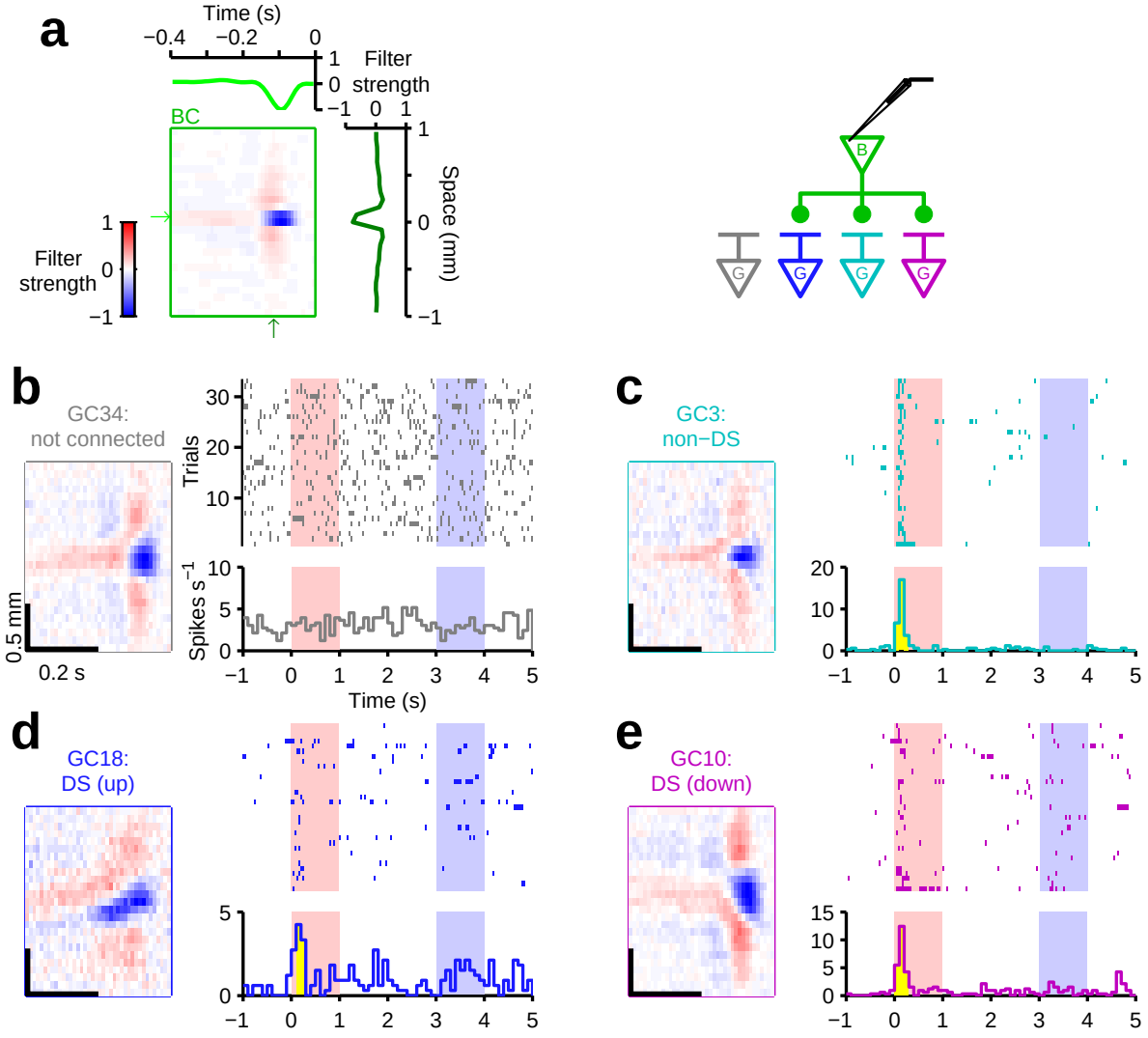

Supplementary Figure 1: Ganglion cells with distinct visual response characteristics receive inputs from the same bipolar cell.

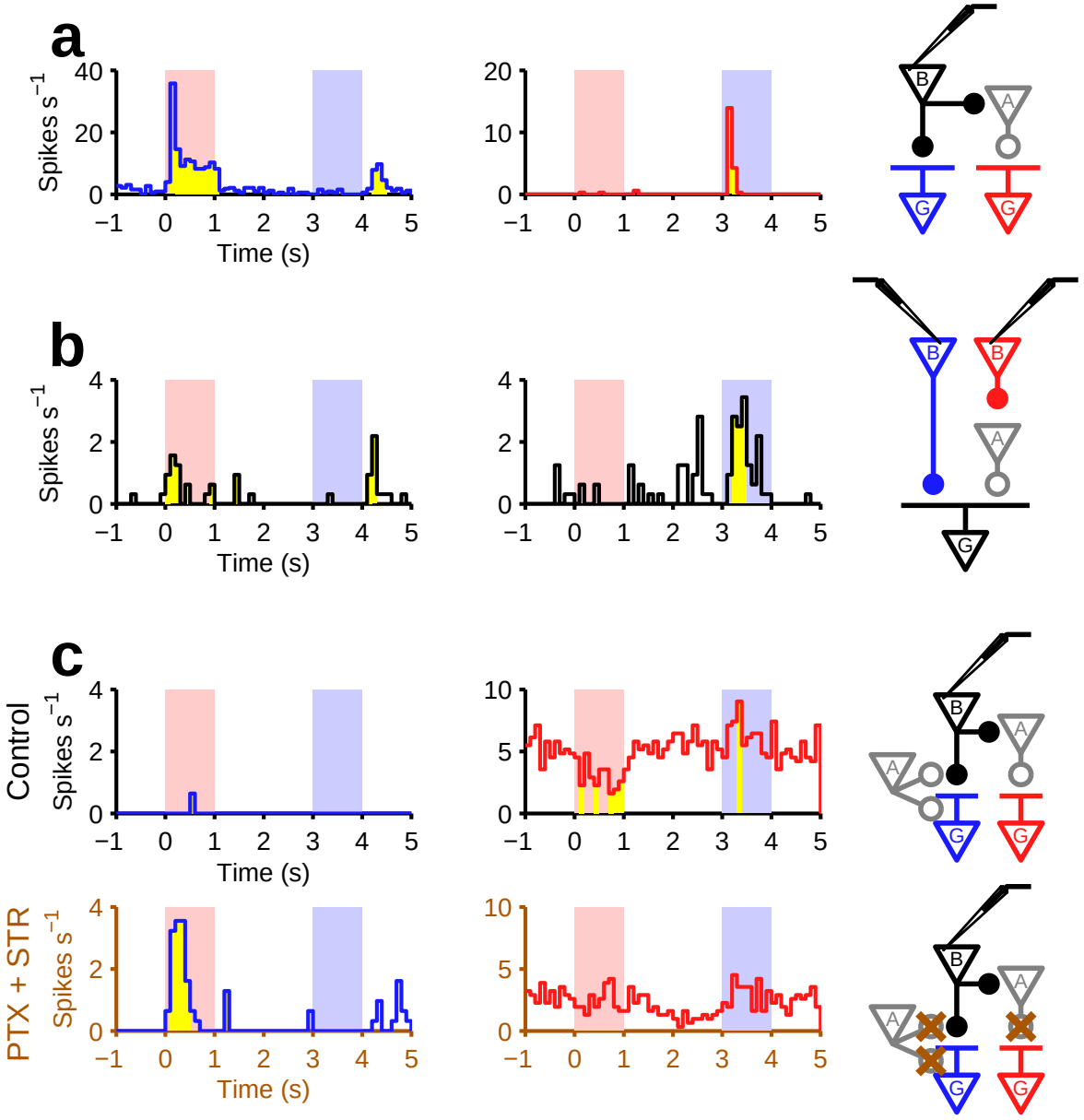

Supplementary Figure 2: Circuits of opposite polarity diverge from single bipolar cells.

Nature Neuroscience: doi:10.1038/nn.3241

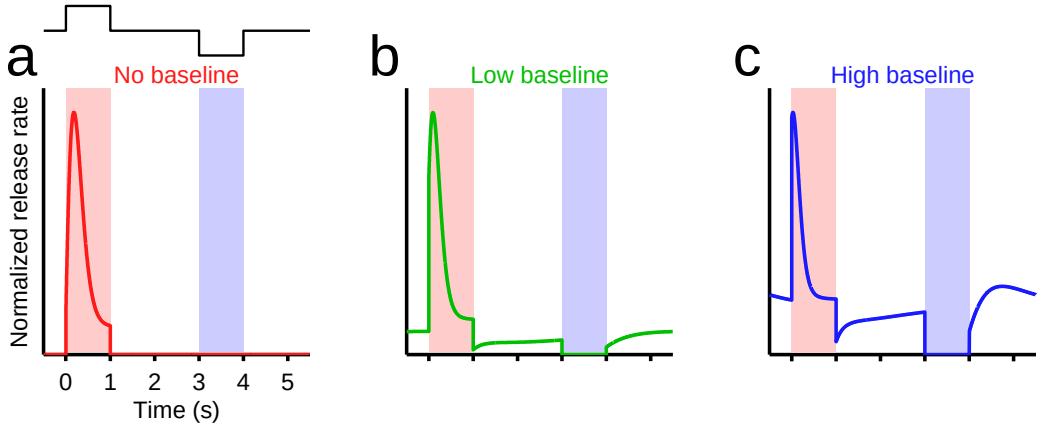

Supplementary Figure 3: Baseline release rate can control the rectification and rebound responses.

Nature Neuroscience: doi:10.1038/nn.3241

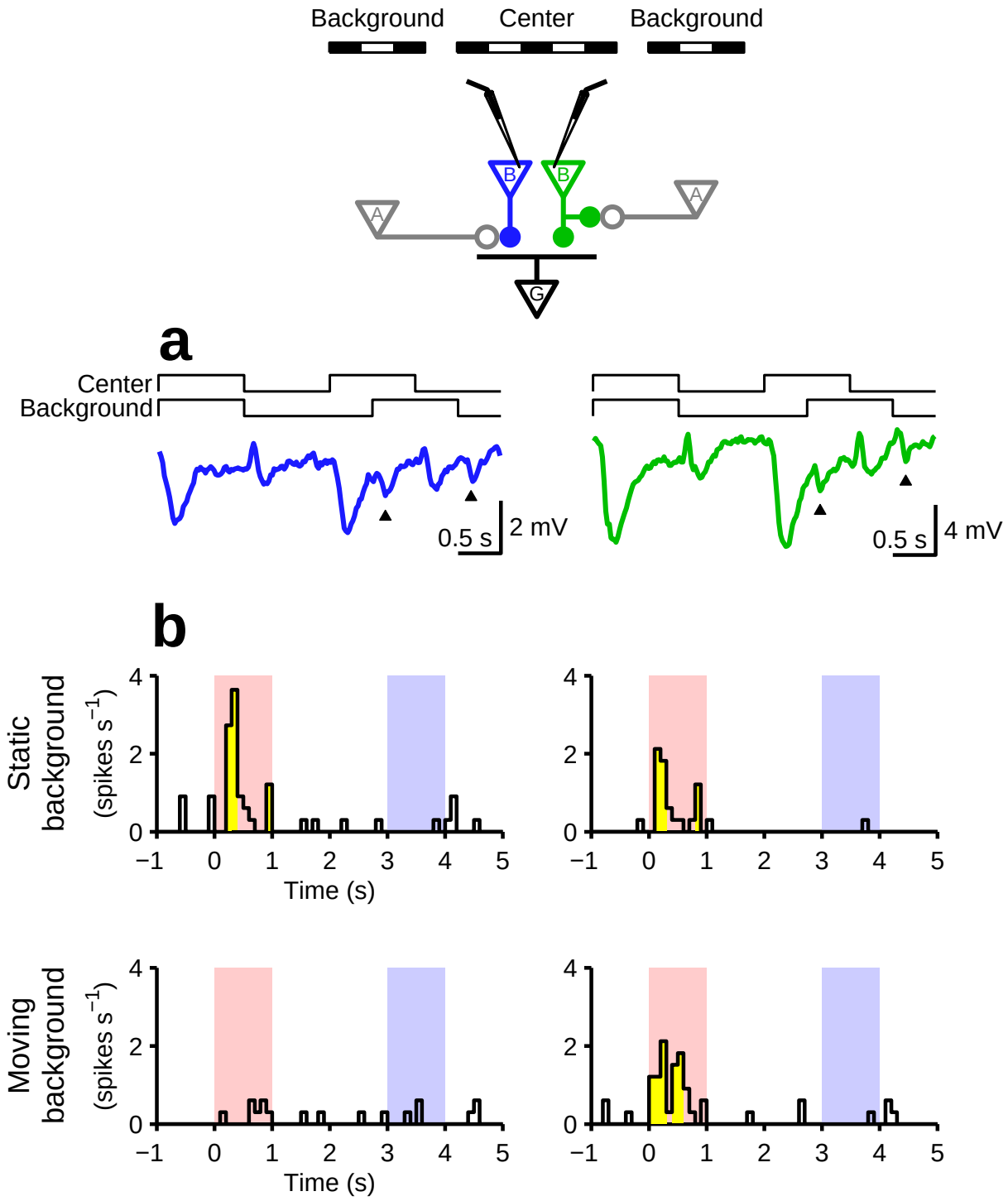

Supplementary Figure 4: Individual bipolar cell terminals are gated presynaptically.

Nature Neuroscience: doi:10.1038/nn.3241

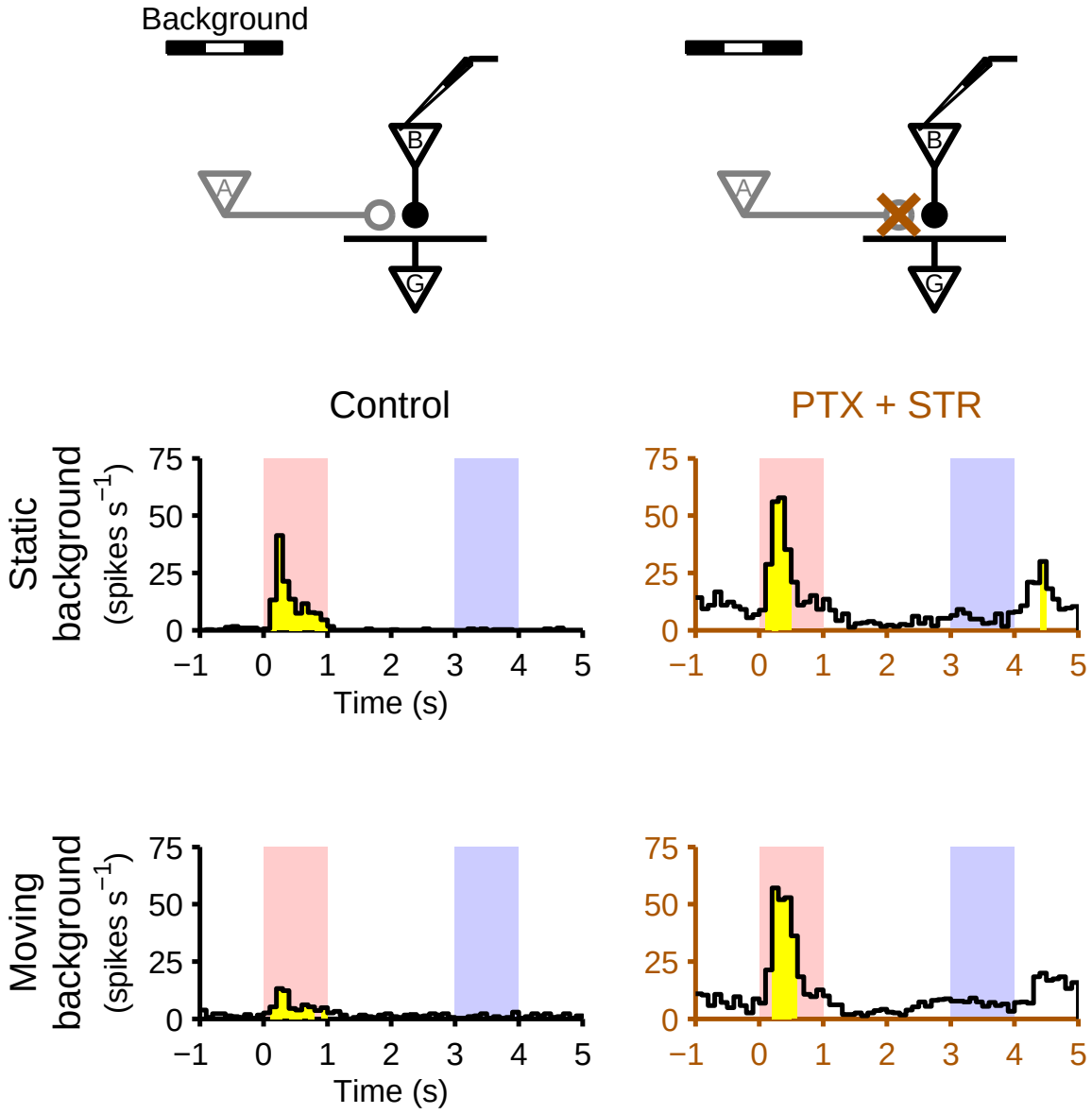

Supplementary Figure 5: Amacrine cells mediate the effects of background visual stimulation on bipolar cell signal transmission.

Nature Neuroscience: doi:10.1038/nn.3241

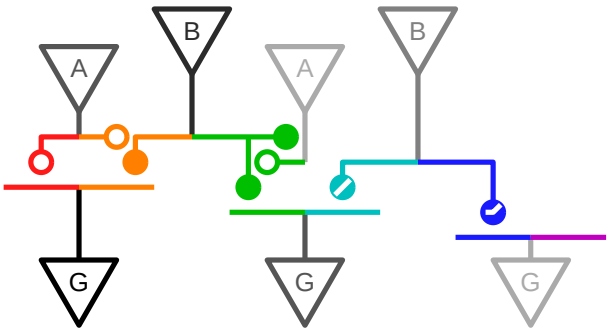

Supplementary Figure 6: Connections between bipolar and ganglion cells form diverse components in the circuit of the retina.

Nature Neuroscience: doi:10.1038/nn.3241

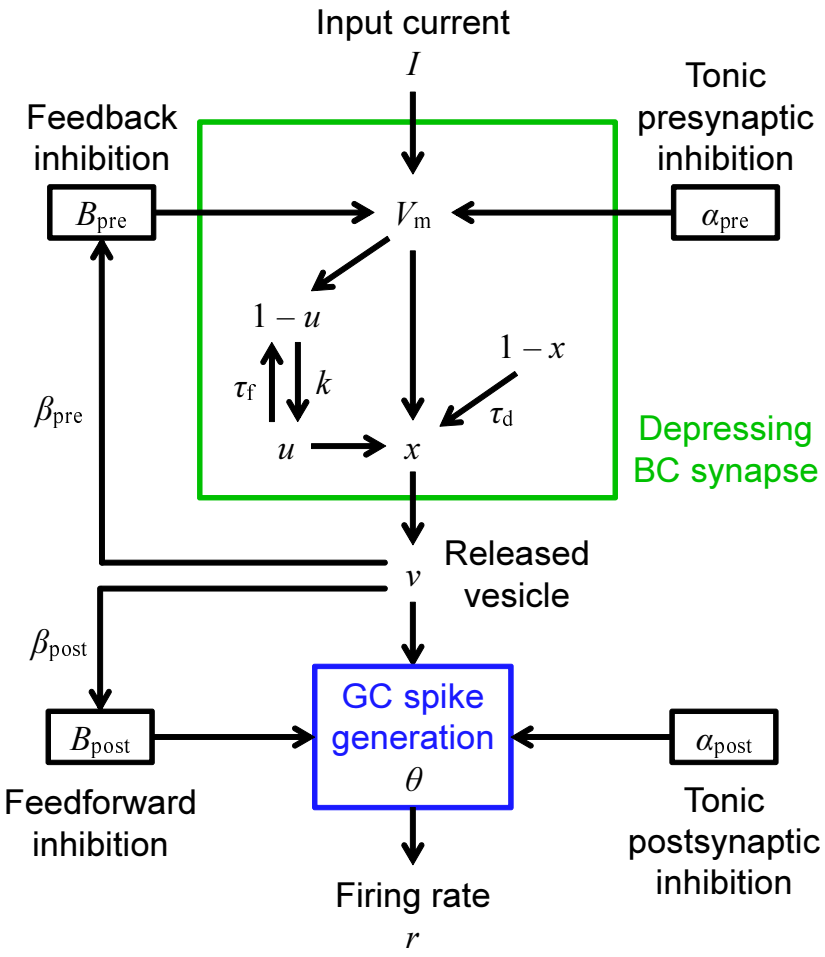

Supplementary Figure 7: Circuit diagram of simulated synaptic transmission from bipolar to ganglion cells.

Nature Neuroscience: doi:10.1038/nn.3241